Solid Earth, 14, 1031–1052, 2023
https://doi.org/10.5194/se-14-1031-2023

Solid Earth Open Access EGU

Mineralogical and elemental geochemical characteristics of Taodonggou Group mudstone in the Taibei Sag, Turpan–Hami Basin: implication for its formation mechanism

Huan Miao[1,2], Jianying Guo[3], Yanbin Wang[4], Zhenxue Jiang[1,2], Chengju Zhang[1,2], and Chuanming Li[1,5]

[1]State Key Laboratory of Oil and Gas Resources and Exploration, Beijing 102249, China
[2]Institute of Unconventional Oil and Gas Science and Technology, China University of Petroleum-Beijing, Beijing 102249, China
[3]CNPC Key Laboratory of Natural Gas Accumulation and Development, Langfang 065007, China
[4]College of Geosciences and Surveying Engineering, China University of Mining and Technology-Beijing, Beijing 100083, China
[5]College of Geosciences, China University of Petroleum-Beijing, Beijing 102249, China

Correspondence: Huan Miao (1627765379@qq.com) and Jianying Guo (gjy_17711224@petrochina.com.cn)

Received: 11 December 2022 – Discussion started: 7 February 2023
Revised: 29 July 2023 – Accepted: 15 August 2023 – Published: 21 September 2023

Abstract. Organic matter types in the Taodonggou Group mudstone exhibit significant differences with depth. In order to understand the formation mechanism of this special phenomenon, we analyzed the mineralogy and geochemistry of the mudstone, as well as the source rocks, depositional environment, and depositional processes of the Taodonggou Group. Based on this, we have gained the following insights. (1) The Taodonggou Group mudstone was deposited in an intermediate-depth or deep, dysoxic, freshwater–brackish lake environment under warm and humid paleoclimatic conditions. The input of terrestrial debris was stable, but the sedimentation rate was slow. In addition, the sedimentation in the middle stage was influenced by hydrothermal activities, and the changes in the depositional environment corresponded to variations in organic matter types. (2) The source rocks of the Taodonggou Group mudstone are mainly andesitic and feldspathic volcanic rocks. Sediment sorting and recycling were weak, and hydrocarbon source information was well preserved. The tectonic background of the source area was a continental island arc and an oceanic island arc. Furthermore, changes in the provenance of the Taodonggou Group also had a significant impact on the variations in organic matter types. (3) The sedimentation of the Taodonggou Group involved both traction and gravity flows. The variations in source area, depositional environment, and depositional processes during different depositional periods led to changes in the organic matter types of the Taodonggou mudstone. (4) Based on the depositional environment, provenance, and depositional processes, the sedimentation of the Taodonggou Group can be divided into three stages. In the early stages, the sedimentation center was in the Bogda area. At this time, the Bogda Mountain region was not exposed, and the depositional processes inherited the characteristics of early Permian gravity flow sedimentation, resulting in the widespread deposition of a series of high-quality Type III source rocks in the basin. In the middle stage of the Taodonggou Group sedimentation, the sedimentation center gradually migrated to the Taibei Sag. During this period, the Bogda Mountain region experienced uplift and hydrothermal activity, and the depositional processes gradually transitioned to traction flows, resulting in the widespread deposition of a series of Type II source rocks in the basin. In the late stage of the Taodonggou Group, the uplift of the Bogda Mountain region ceased, and the sedimentation center completely shifted to the Taibei Sag. Meanwhile, under the influence of gravity flows, the organic matter types of the Taodonggou mudstone changed to Type III.

Published by Copernicus Publications on behalf of the European Geosciences Union.

1 Introduction

Turpan–Hami Basin, Junggar Basin, and the Bogda area all belong to the southern part of the ancient Asian Ocean in the Paleozoic era (Korobkin and Buslov, 2011; Jiang et al., 2015). During the early Carboniferous to early Permian, they began momentously to separate due to the continuous expansion of the Bogda Rift and began to enter the basin-forming period in the middle Permian (Miao et al., 2004; Novikov, 2013; Jiang et al., 2015; J. Wang et al., 2019; S. Zhang et al., 2019). The middle Permian is a momentous stage in the tectonic evolution of the Turpan–Hami Basin. During this period, the expansion of the Bogda Rift stopped. With the gradual withdrawal of seawater from Xinjiang, the sedimentary environment of the Turpan–Hami Basin gradually shifted to continental facies, and the sedimentary center gradually shifted from the Bogda area to the Taibei Sag (Miao et al., 2004; Shi et al., 2020; Li et al., 2022). Taodonggou Group mudstones are widely deposited in the Turpan–Hami Basin. Previous studies have confirmed that Taodonggou Group mudstone is a very good to excellent source rock with huge hydrocarbon generation potential (Song et al., 2018; Miao et al., 2021, 2022a, b). It has been found that the organic matter types of the Taodonggou mudstone can be classified into two categories, with the upper and lower sections being Type III and the middle section being Type II (Miao et al., 2021, 2023).

The hydrocarbon generation potential of mudstone is closely related to its sedimentary environment (Wu et al., 2021; Li et al., 2022; K. Zhang et al., 2019; Zhao et al., 2021; Miao et al., 2004). Regarding the sedimentary environment of the Taodonggou Group mudstone, previous researchers have conducted extensive research. Miao et al. (2004) believed that the mudstone in the Taodonggou Group was deposited in a warm and humid paleoclimate, high-salinity waterbodies, and an anoxic environment. Yang et al. (2010), based on the sedimentary characteristics of the Taerlang Formation and the Daheyan Formation, believed that the Taodonggou Group was deposited in a subhumid climate and that climate change is periodic. Wei (2015) also confirmed that the paleoclimate change in the Taodonggou Group stratum has a cyclical feature through tree rings and is mainly a warm and humid paleoclimate. At the same time, Song et al. (2018) also confirmed this by using the elemental geochemical characteristics of the Taodonggou Group shale outcrops in the field. Tian et al. (2017) analyzed the biomarkers of the Taodonggou Group in seven outcrops around the Turpan–Hami Basin and concluded that the mudstone of the Taodonggou Group was deposited in a balanced, filled lake with little or no terrestrial organic matter; a large amount of algal organic matter input; and weakly alkaline, hypoxic to hypoxic brackish water. Miao et al. (2021) found biomarkers in the Taodonggou Formation mudstone from wells YT1 and L30 from different perspectives of Tian et al. (2017), which may be related to the weathering effect of outcrop samples. Through the research of the above scholars, we have found that there is some controversy over the sedimentary environment of the Taodonggou Group, and the relationship between the cyclic changes in the sedimentary environment and the changes in the organic matter types of the Taodonggou Group mudstone is still unclear.

In addition, the provenance and sedimentation mode of sediments also have a significant influence on the organic matter types in mudstones (Mei et al., 2020). Mudstone belongs to a category of fine-grained sediment that is challenging to analyze using traditional heavy-mineral analysis methods (Rollinson, 1993; Roser and Korsch, 1988; Gehrels et al., 2008). Therefore, elemental geochemical methods can be employed for provenance analysis (McLennan et al., 1983; Taylor and McLennan, 1985; Li et al., 2020). Elemental geochemical analysis compares the major, trace, and rare-earth element characteristics of mudstones in the sedimentary area with those of lithologies in the provenance area to determine the lithology of source rocks, weathering degree, and tectonic background of the sediment source area (Li et al., 2020; Floyd and Leveridge, 1987; Basu et al., 2016). Previous studies have found that the sediment source not only affects variations in the salinity of lake water but also influences the input of nutrients and terrestrial organic matter, thus impacting the quality of mudstones (Li et al., 2020; Deditius, 2015; Essefi, 2021). The tectonic activity in the source area not only affects changes in the sedimentary center but also influences the source area (Miao et al., 2022c; Pinto et al., 2010). Therefore, reconstructing the location and sedimentation mode of the sediment source area is of great significance for understanding the variations in organic matter types in the Taodonggou Group mudstones.

Based on the mineralogical and elemental geochemical characteristics of 16 mudstone samples collected from well YT1, this study aims to reconstruct the paleoclimatic features, provenance, and tectonic background of the sedimentary period in the source area of the Taodonggou Group mudstones. It also aims to explore the influence of sedimentary environment, provenance changes, and sedimentation mode on the deposition of the Taodonggou Group mudstones in order to reveal the formation process of the mudstones.

2 Geological setting

The Turpan–Hami Basin, located in the eastern part of the Xinjiang Uygur Autonomous Region, is one of the three major petroliferous basins in Xinjiang. It is 660 km long from east to west and 130 km wide from north to south, with a total covered area of $5.35 \times 104\,km^2$. The Turpan–Hami Basin has undergone four stages: the extensional rift basin development stage; the compressional foreland basin development stage; the extensional faulted basin development stage; and the compressional regenerated foreland basin development stage, which finally formed the current pattern of the

Mesozoic–Cenozoic superimposed composite inland basin (Zhu et al., 2009; Jiang et al., 2015; Wartes et al., 2002; Greene et al., 2005). According to the tectonic evolution characteristics of the Turpan–Hami Basin, the Turpan–Hami Basin can be divided into three primary tectonic units from east to west: the Hami Depression, the Liaodun Uplift, and the Turpan Depression (Miao et al., 2021; Fig. 1a).

Taibei Sag, the secondary sag of the Turpan Depression in the Turpan–Hami Basin, is the largest sedimentary unit in the Turpan–Hami Basin (Fig. 1b). The Taibei Sag is a Paleozoic–Cenozoic-inherited subsidence area (Li et al., 2021), which is a key area for oil and gas exploration in the Turpan–Hami Basin due to its high degree of thermal evolution of hydrocarbon source rocks; good physical reservoir properties; good cap sealing; and rich oil and gas resources, which are the focus of oil and gas exploration in the Turpan–Hami Basin (Wu et al., 2021; Li et al., 2021). The Taodonggou Group is the general name of the Daheyan Formation and the Taerlang Formation. The Daheyan Formation is composed of a sequence of sandstone and conglomerate deposits, with locally interbedded gray to dark-gray mudstone. It is unconformably overlain by the Yierxitu Formation. The Taerlang Formation is predominantly composed of gray–black mudstone, with localized occurrences of gray–green siltstone and medium-grained sandstone. Due to the fact that the stratigraphic boundary between the Taerlang Formation and the Daheyan Formation is not obvious, they are collectively called the Taodonggou Group. The middle Permian Taodonggou Group is mainly located in the western part of the study area. At present, only wells YT1 and L30 are drilled (well YT1 is drilled through; well L30 is not drilled through). The burial depth of the stratum is 4000–6500 m, and the thickness of the mudstone is 50–200 m (Miao et al., 2022c).

3 Samples and experiments

3.1 Samples

In this study, 16 mudstone samples were collected from well YT1, numbered YT1-1 to YT1-16 in order of depth. After cleaning the samples, X-ray diffraction (XRD), X-ray fluorescence spectrometer (XRF), and inductively coupled plasma mass spectrometer (ICP-MS) experiments were conducted.

3.2 Experiments

The XRD experiment was carried out at Hangzhou Yanqu Information Co., Ltd. The experimental instrument was the Ultima VI XRD testing instrument of Rigaku Corporation. In accordance with the Chinese industry standard SY/T 5163-2018, the mudstone was broken to a particle size of fewer than 200 meshes, and 2 g of samples was weighed to obtain XRD images through Cu / Ka radiation at a scanning speed of $2^\circ\,\mathrm{min}^{-1}$. The measurement angle range was $3^\circ \le 2\theta \le 70^\circ$, and finally, quantitative interpretation is made with the software X'Pert HighScore Plus of Malvern Panalytical.

The XRF experiment was conducted at Hangzhou Yanqu Information Co., Ltd., and the experimental instrument was a Malvern Panalytical Axios tester. The mudstone was first crushed to a particle size of fewer than 200 meshes. Then 10 g of the sample was weighed and calcined in a muffle furnace for 4 h to get rid of organic matter and carbonates, and the weight loss was recorded. Finally $Li_2B_4O_7$ was added, mixed evenly, and made into glass bead, and the main element concentration was tested.

The ICP-MS test was performed at Beijing Orient Smart, and the test instrument was an Element XR inductively coupled plasma emission spectrometer manufactured by Thermo Fisher, Inc. Before analysis, the samples were ground to a particle size of less than 40 µm. An appropriate amount of the sample was weighed and dissolved in HF (30 %) and HNO_3 (68 %) at 190 °C for 24 h. After evaporating the excess solvent with deionized water, the solution was redissolved in 2 mL of 6.5 % HNO_3 and then stored at 150 °C for 48 h. Subsequently, after evaporating the solution, 1 mL of the 6 mol L^{-1} HNO_3 evaporated solution was added to the sample.

4 Results

4.1 Mineralogy

The XRD test results of 16 samples from well YT1 are shown in Table A1 and Fig. 2. As can be seen from Table A1 and Fig. 2, Taodonggou Group mudstones are composed of clay, quartz, calcite, plagioclase, baryte, and *K*-feldspar, and some samples contain siderite and pyrite. The content of clay is the highest (23.9 %–70.9 %, mean = 40.78 %), followed by quartz (17.2 %–59.2 %, mean = 34.69 %), calcite (1 %–35.4 %, mean = 16.97 %), baryte (0 %–13.3 %, mean = 4.21 %), plagioclase (0 %–5.4 %, mean = 2.93 %), and *K*-feldspar (0 %–2.3 %, mean = 0.9 %).

The mineral composition can be used to analyze the lithofacies type of mudstone, and different lithofacies types often have different characteristics (Glaser et al., 2014). Previous scholars believed that mudstone types could be divided by the ternary diagram of mineral composition. The three end elements of the ternary diagram are quartz + feldspar + mica (QFM), calcite + dolomite + ankerite + siderite + magnesite (carbonate), and clay. The XRD results of 16 mudstone samples from well YT1 in the study area are put into the ternary map (Fig. 3). The results show that the data points of Taodonggou Group mudstone in the study area are located in four areas, namely mixed mudstone, silica-rich argillaceous mudstone, argillaceous siliceous mudstone, and mixed siliceous mudstone, and most of the points are mixed mudstone and argillaceous siliceous mudstone areas, which indi-

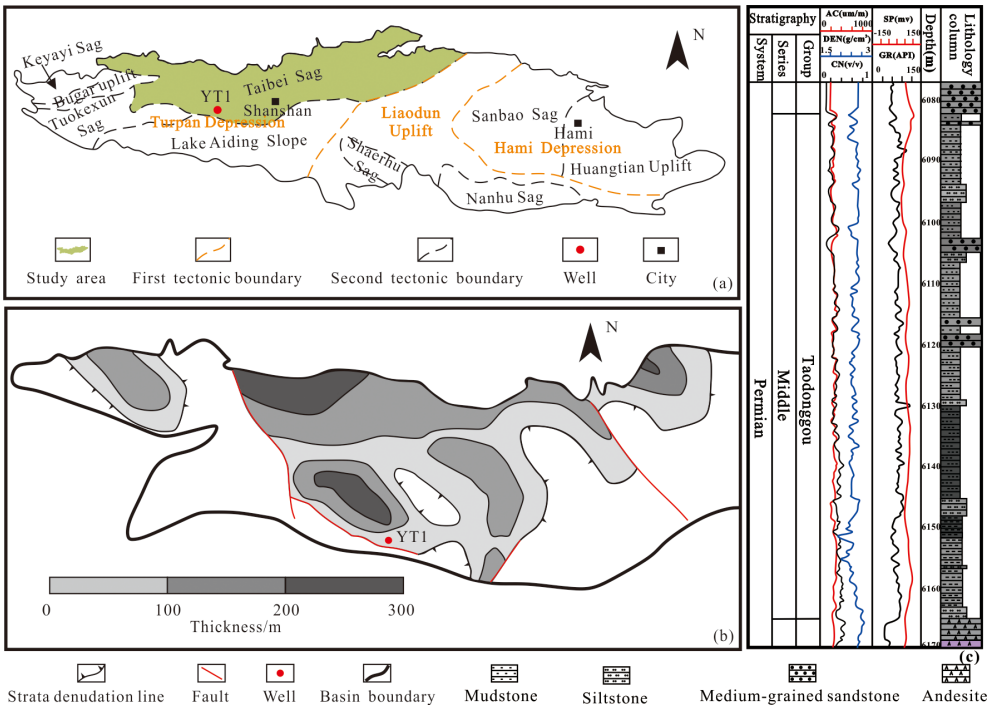

Figure 1. Geological overview of the study area (modified after Miao et al., 2021, 2023): **(a)** geological background of the Turpan–Hami Basin, **(b)** thickness contour map of Taodonggou Group mudstone in the Taibei Sag, **(c)** YT1 stratum of the Taodonggou Group.

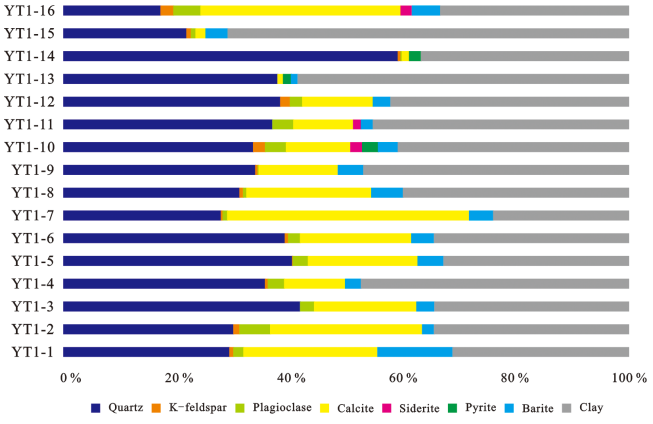

Figure 2. Mineral composition of Taodonggou Group mudstone in well YT1.

cates that Taodonggou Group mudstone can be divided into four types – mixed mudstone, silica-rich argillaceous mudstone, argillaceous siliceous mudstone, and mixed siliceous mudstone – and the main lithofacies are mixed mudstone and argillaceous siliceous mudstone.

4.2 Major element

Table A2 shows the results of the major elements in 16 mudstone samples from well YT1. From Table A2, we can see that the major elements of the Taodonggou Group mudstone are mainly SiO_2, Al_2O_3, Fe_2O_3, CaO, and TiO_2. The highest content of SiO_2 is from 43.11 %–70.11 %, with an average value of 56.18 %. Al_2O_3 content takes second place, accounting for 11.65 % to 25.75 %, with an average value of 18.69 %; the average content of another main element is less than 10 %.

4.3 Trace element

The trace element content of the Taodonggou Group mudstone is shown in Table A3. The enrichment factor (EF) is an important indicator of element enrichment (Taylor and McLennan, 1985; Ross and Bustin, 2009). By comparing the trace element content of the mudstone of the Taodonggou Group with the global average shale (AS), the trace element enrichment factors in the study area are calculated as follows:

$$X_{\mathrm{EF}} = \frac{(X/\mathrm{Al})_{\mathrm{samples}}}{(X/\mathrm{Al})_{\mathrm{AS}}}, \quad (1)$$

where X and Al represent the concentrations of elements X and Al (Taylor and McLennan, 1985; Ross and Bustin, 2009). $X_{\mathrm{EF}} < 1$ represents the dilution concentration of element X relative to the standard composition, $X_{\mathrm{EF}} > 1$ represents the relative enrichment of element X compared to the AS concentration, $X_{\mathrm{EF}} > 3$ represents the detectable autogenetic enrichment, and $X_{\mathrm{EF}} > 10$ is considered an indicator of moderate to strong autogenetic enrichment (Taylor and McLennan, 1985; Ross and Bustin, 2009).

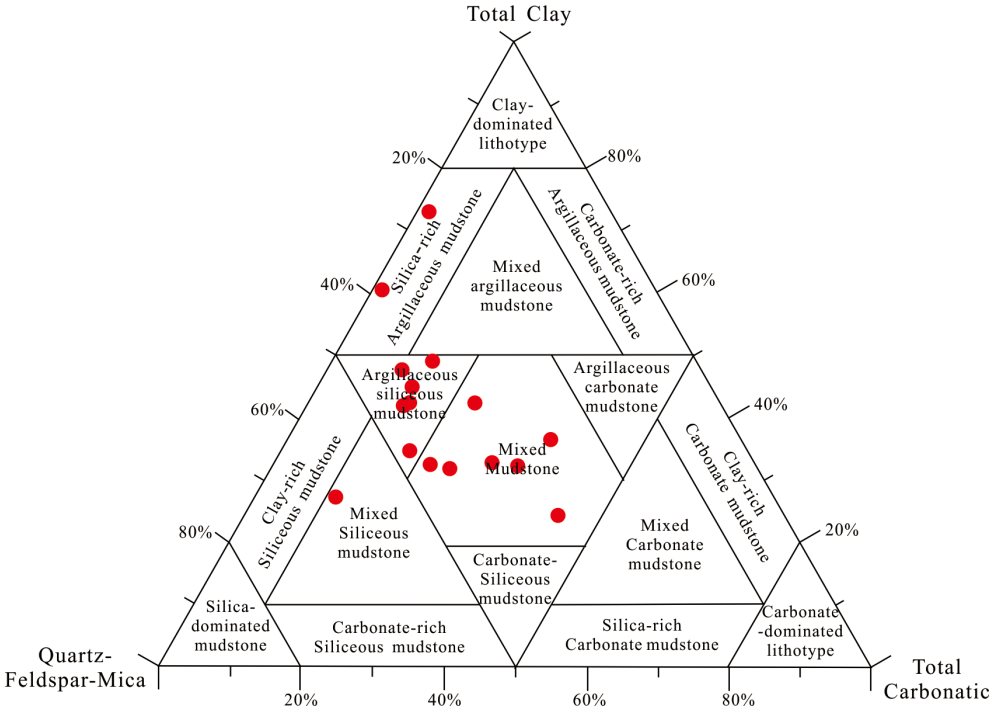

Figure 3. Lithofacies classification of Taodonggou Group mudstone in well YT1 (modified from Glaser et al., 2014).

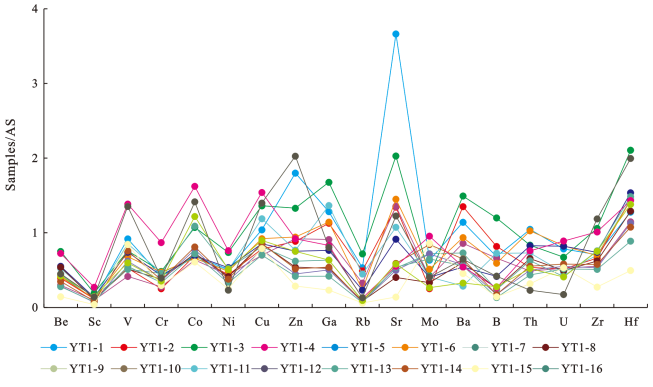

Figure 4. AS standardized multi-element diagrams of Taodonggou Group mudstone in the study area.

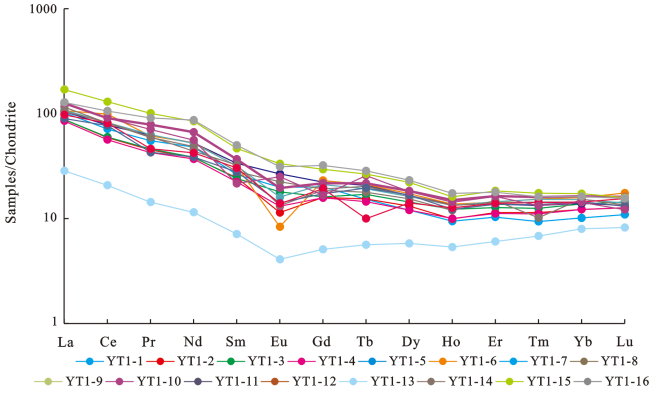

Figure 5. Standardized map of rare-earth element chondrite in mudstone of the Taodonggou Group.

Figure 4 and Table A4 present the enrichment factors of Taodonggou Group mudstone in the study area. It can be seen from Fig. 4 and Table A4 that only Hf (0.5–2.11, mean = 1.29) is enriched in the Taodonggou Group mudstone compared with AS, and other elements are not enriched.

4.4 Rare-earth element

The rare-earth element (REE) content of Taodonggou Group mudstone in the study area is shown in Table A5. According to Table A5, the $\sum$REE content of Taodonggou Group mudstone ranged from 43.247 to 257.997 ppm, with an average value of 159.206 ppm. The light rare-earth element (LREE) content was the highest (mean value = 133.45 ppm), followed by medium rare-earth element (MREE) (mean value = 17.438 ppm) and heavy rare-earth element (HREE) (mean value 6.684 ppm) in that order. After chondrite standardization (Taylor and Mclennan, 1985), Taodonggou Group mudstone shows a right-dipping REE distribution pattern (Fig. 5); $(La/Yb)_N$ is 6.228–10.081, with an average value of 7.358.

In addition, in Fig. 5, although the YT1-13 sample exhibits a weak right-dipping REE distribution pattern similar to other samples, its rare-earth elements are significantly de-

pleted. Based on Fig. 4 and Table A4, the trace elements in the YT1-13 sample are depleted compared to AS, indicating that the YT1-13 sample has been influenced by groundwater leaching.

4.5 Reconstruction of paleosedimentary environment based on elemental geochemical characteristics

4.5.1 Paleoclimate and weathering

The paleoclimate affects not only the weathering degree of the parent rock but also the transport distance of sedimentary debris and the transport of nutrients (Zhang et al., 2005). There are many evaluation indices for paleoclimate, such as the chemical-alteration index (CIA) and the climate index (C). It is generally believed that CIA = 50–65 and $C < 0.2$ reflect that the sedimentary system is in a dry and cold climate against the background of a lower degree of chemical weathering, CIA = 65–85 and $0.2 < C < 0.8$ indicate that the sedimentary system is in a warm and humid climate against the background of a medium degree of chemical weathering, and CIA = 85–100 and $C > 0.8$ reflect the humid and hot climate against the background of a high degree of chemical weathering (Zhang et al., 2019; Nesbitt and Young, 1984). The calculation formula for CIA and C is as follows:

$$\mathrm{CIA} = \frac{\mathrm{Al_2O_3} \times 100}{\mathrm{Al_2O_3} + \mathrm{Na_2O} + \mathrm{CaO^*} + \mathrm{K_2O}} \quad (2)$$

$$C = \frac{\mathrm{Fe} + \mathrm{Mn} + \mathrm{Cr} + \mathrm{Ni} + \mathrm{V} + \mathrm{Co}}{\mathrm{Ca} + \mathrm{Mg} + \mathrm{Sr} + \mathrm{Ba} + \mathrm{K} + \mathrm{Na}}. \quad (3)$$

In Eq. (2), $\mathrm{CaO^*}$ only refers to CaO in silicate minerals. Due to the lack of direct measurement means, it is often calculated indirectly by the content of $\mathrm{P_2O_5}$, namely

$$\mathrm{CaO^*} = \mathrm{mol(CaO)} - \frac{10}{3}\mathrm{mol\,(P_2O_5)}, \quad (4)$$

where mol(CaO) and mol($\mathrm{P_2O_5}$) are the mole numbers of CaO and $\mathrm{P_2O_5}$, where when mol ($\mathrm{Na_2O}$) ≤ mol ($\mathrm{CaO^*}$), mol ($\mathrm{CaO^*}$) = mol ($\mathrm{Na_2O}$); in contrast, when mol($\mathrm{Na_2O}$) > mol($\mathrm{CaO^*}$), mol($\mathrm{CaO^*}$) = mol(CaO) (Nesbitt and Young, 1984). The CIA values of the Taodonggou Group mudstone in the study area were calculated based on Eqs. (2) and (3), ranging from 68.71 to 96.97, with a mean value of 80.17. The climate index (C) is 0.22–2.42 (average = 1.01; Table 3). The overall paleoclimate was warm, humid, and hot (Fig. 6a).

In addition, the cross-plot of Ga / Rb and $\mathrm{K_2O}$ / $\mathrm{Al_2O_3}$ can also be used to analyze the paleoclimate characteristics during the formation of sedimentary rocks (Lerman and Baccini, 1987; Liu and Zhou, 2007). As shown in the cross-plot of Ga / Rb and $\mathrm{K_2O}$ / $\mathrm{Al_2O_3}$ (Fig. 6b), almost all points are in the warm/wet area, which indicates that Taodonggou Group mudstone was deposited in a warm and humid paleoclimate.

By analyzing the correlations between CIA, C, and Ga / Rb (Fig. 6c–e), it can be observed that there is the strongest correlation between CIA and C (Fig. 6c; $R^2 = 0.7566$). Additionally, the correlation coefficients between CIA and Ga / Rb and between C and Ga / Rb are both greater than 0.4 (Fig. 6d and e). This indicates that CIA, C, and Ga / Rb are reliable indicators of the paleoclimate during the sedimentation of the Taodonggou Group mudstone. Based on the above analysis, the Taodonggou Group mudstone in the study area was deposited in a warm, humid, and hot paleoclimate. This result is consistent with Miao's indicator result using the biomarker parameter CPI (carbon advantage index) (Miao et al., 2021), indicating that the biomarker parameter CPI can be used to explain the paleoclimate change characteristics of hydrocarbon source rocks with Ro ≤ 1.49.

4.5.2 Paleoredox conditions

Redox environments are critical to the preservation of organic matter in sedimentary rocks, and sensitive elements such as Co, Mo, U, Th, V, Ni, and Cr are commonly used to identify redox conditions in ancient waterbodies. Previous evidence suggests that U / Th < 0.75, V / Cr < 2, and V / (V + Ni) < 0.45 represent oxic conditions; 0.75 < U / Th < 1.25, 2 < V / Cr < 4.25, and 0.45 < V / (V + Ni) < 0.84 represent dysoxic conditions; and U / Th < 1.25, V / Cr < 4.25, and V / (V + Ni) < 0.84 represent anoxic conditions (Hatch and Leventhal, 1992; Rosenthal et al., 1995; Tribovillard et al., 2006, 2012). There is no significant correlation between V, U, and Th and $\mathrm{Al_2O_3}$ contents in the Taodonggou Group mudstone samples, indicating that V, U, and Th contents in Taodonggou Group mudstone are mainly controlled by authigenic deposition under redox conditions (Tribovillard et al., 1994). The U / Th, V / Cr, and V / (V + Ni) of the Taodonggou Group mudstone range from 0.21 to 0.52 (mean = 0.29), 1.62 to 4.95 (mean = 2.7), and 0.65 to 0.92 (mean = 0.75). In light of U / Th, Taodonggou Group mudstones were deposited in an oxic environment, and according to V / Cr and V / (V + Ni), Taodonggou Group mudstones were deposited in a dysoxic environment. This is because U / Th cannot accurately identify the redox environment of the sediments under highly weathered conditions (Cao et al., 2021), so V / Cr and V / (V + Ni) were used in this study to identify the redox environment of Taodonggou Group mudstone. The cross-plot of V / Cr and V / (V + Ni) shows (Fig. 7) that Taodonggou Group mudstones were deposited in a dysoxic environment.

4.5.3 Paleosalinity

Paleosalinity is an important indicator of the paleoenvironment of a water body. The level of paleosalinity affects the stratification of the sedimentary waterbody and the development of plankton, thereby affecting the paleoproductivity and enrichment of organic matter in the sedimentary environment (Thorpe et al., 2012; Wang et al., 2021; Shi et al., 2021). Previous research has found that Sr / Ba and B / Ga

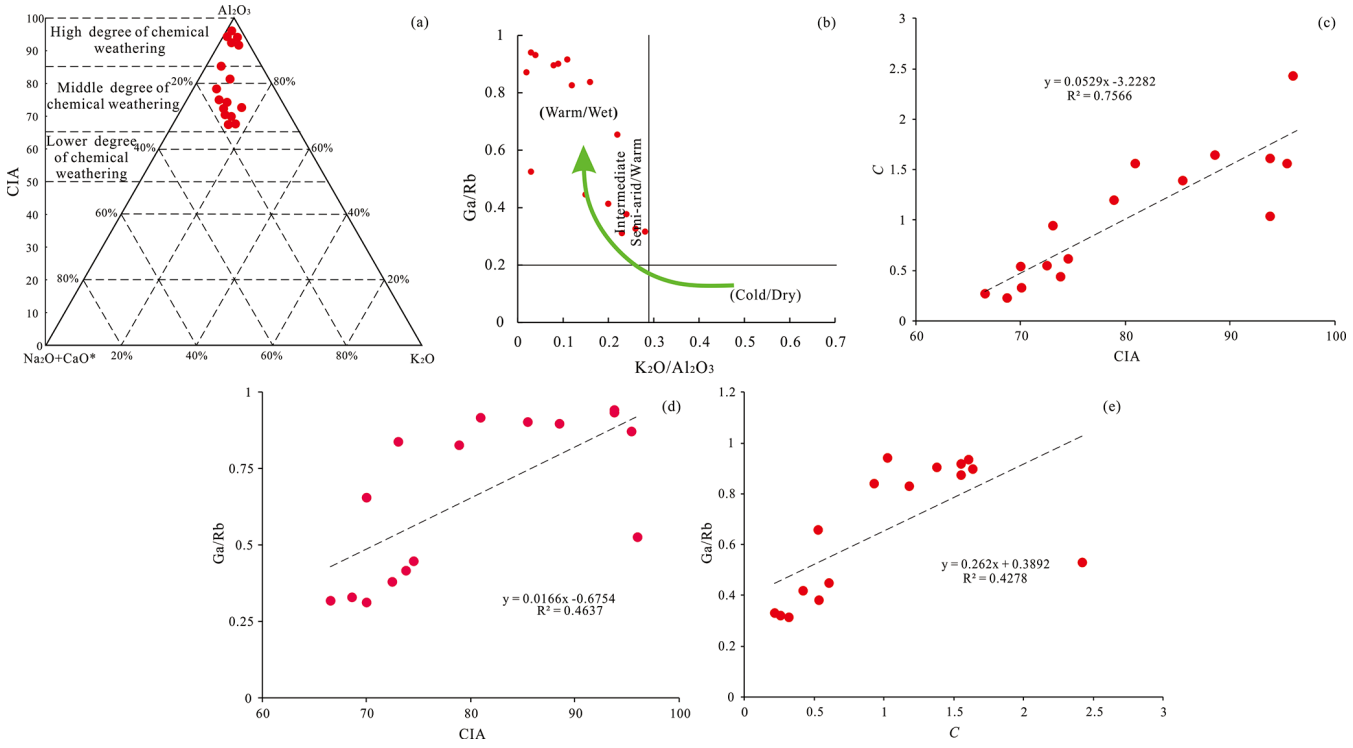

Figure 6. Paleoclimate of the Taodonggou Group: **(a)** CIA characteristics of Taodonggou Group mudstone (modified from Nesbitt and Young, 1984), **(b)** cross-plot of K_2O / Al_2O_3 and Ga / Rb (modified from Roy and Roser, 2013), **(c)** cross-plot of CIA and *C*, **(d)** cross-plot of CIA and Ga / Rb, **(e)** cross-plot of *C* and Ga / Rb.

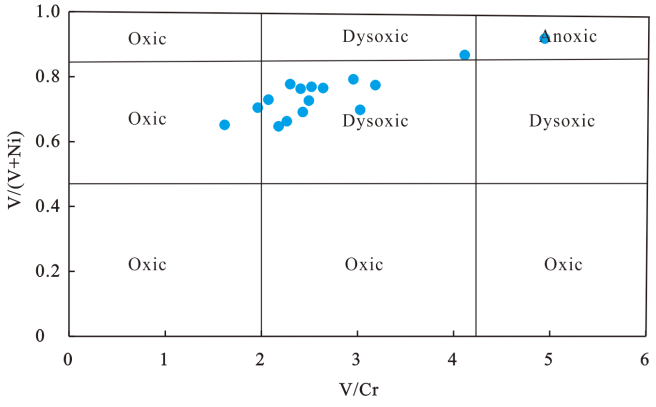

Figure 7. Cross-plot of V / Cr and V / (V + Ni).

can represent changes in paleosalinity. It is generally believed that Sr / Ba < 0.5 or B / Ga < 3 represents fresh water, 0.5 < Sr / Ba < 1 or 3 < B / Ga < 6 means brackish water, and Sr / Ba > 1 or B / Ga > 6 represents saline water. The correlation between Sr and CaO of Taodonggou Group mudstone in the study area is not obvious ($R^2 = 0.17$); Sr / Ba of Taodonggou Group mudstone in the study area ranges from 0.32 to 1.83, with an average value of 0.71, and the B / Ga is 2.53–5.81 (average = 3.36), indicating that Taodonggou Group mudstone was deposited in freshwater and brackish-water environments (Fig. 8a).

In addition, Ca / (Ca + Fe) is a reliable indicator for evaluating the salinity of lake waters (Z. Wang et al., 2021). The Ca / (Ca + Fe) distribution of Taodonggou Group mudstone in the study area ranges from 0.14 to 0.78, with a mean value of 0.42. The Sr / Ba and Ca / (Ca + Fe) intersection diagram (Fig. 8b) shows that Taodonggou Group mudstones were deposited in freshwater and brackish-water environments, which is in accordance with the Sr / Ba and B / Ga intersection diagram.

4.5.4 Paleobathymetry

Previous research has shown that some elements of the sedimentation process change dramatically with offshore distance. These elements can be used to judge the water depth variation during the sedimentation period. The commonly used indicators are Zr / Al, Rb / K, and MnO content (Xiong and Xiao, 2011; Herkat et al., 2013). It is now believed that the lower the Zr / Al ratio or the higher the Rb / K ratio, the further offshore and the deeper the water (Xiong and Xiao, 2011; Herkat et al., 2013). Zr / Al of Taodonggou Group mudstone is 5.19×10^{-4}–22.51×10^{-4} (average = 13.44×10^{-4}), showing first a decreasing and then an increasing trend with the depth; Rb / K ranges from

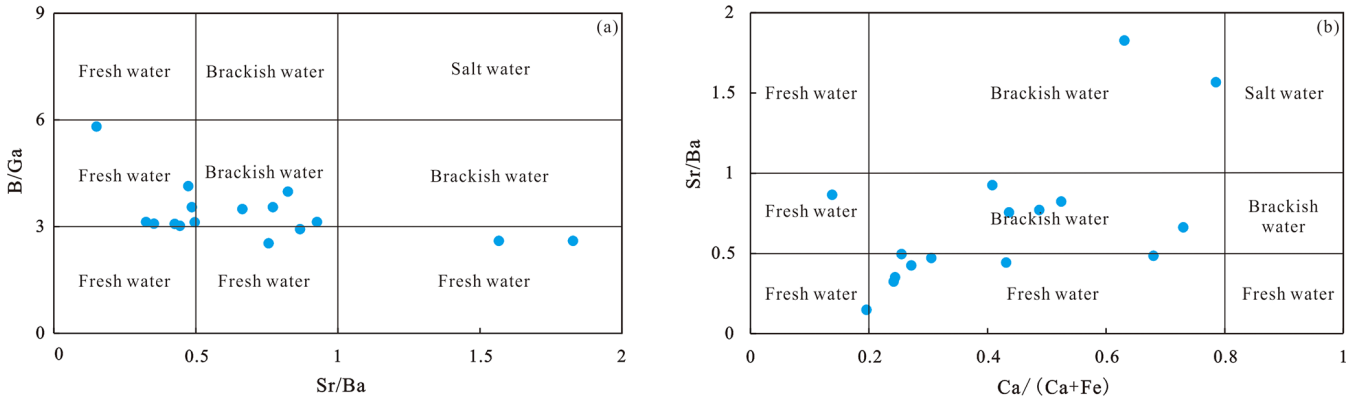

Figure 8. Cross-plot of B / Ga and Sr / Ba **(a)** and cross-plot of Ca / (Ca + Fe) and Sr / Ba **(b)**.

7.32×10^{-4} to 29.79×10^{-4} (mean $= 19.02 \times 10^{-4}$), with large fluctuations with depth of burial. The high-value area of Rb / K is basically consistent with the low-value area of Zr / Al, which indicates that the ancient water depth during the Taodonggou Group mudstone deposition process has first a decreasing and then an increasing trend.

For the content of MnO, it is generally believed that $< 0.00094\,\%$ is a shore lake, $0.00094\,\%$–$0.0075\,\%$ is a shallow lake, $0.0075\,\%$–$0.051\,\%$ is an intermediate-depth lake, and $> 0.051\,\%$ is a deep lake (Herkat et al., 2013). MnO of Taodonggou Group mudstone is $0.05\,\%$–$0.30\,\%$, with an average of $0.16\,\%$, which indicates that the Taodonggou Group mudstone is mainly deposited in an intermediate-depth–deep sedimentary lake environment.

4.5.5 Terrigenous detritus input

Ti, Si, and Al are relatively stable during diagenesis and are usually used as indicators of debris flux input (Algeo and Maynard, 2004; Maravelis et al., 2021). Generally, Ti in sediments comes from ilmenite ($FeTiO_3$) or rutile (TiO_2), while Al can exist in feldspar, clay minerals, and other aluminum silicate minerals (Algeo and Maynard, 2004). Compared with Ti and Al, Si comes from many sources, including sources of biological origin and hydrothermal and terrigenous clastic input (Kidder and Erwin, 2001). Therefore, when using SiO_2 as the evaluation index for terrigenous clastic input, its source needs to be analyzed. The correlation of Al_2O_3 and TiO_2 with SiO_2 in well YT1 of the study area is not obvious, which indicates that their sources are more complex and not dominated by terrestrial debris sources (Fig. 9). Therefore, Al_2O_3 and TiO_2 are used in this study to indicate the terrestrial debris input during the deposition of the Taodonggou Group mudstone.

The Al_2O_3 content of well YT1 is higher, ranging from $11.65\,\%$ to $25.75\,\%$, with an average value of $18.69\,\%$; the TiO_2 is $1.15\,\%$–$4.22\,\%$ (average $= 1.77\,\%$). As can be seen from Table A2, the Al_2O_3 content of well YT1 fluctuates more with depth, and there is first an increasing and then a decreasing trend with depth overall, while the TiO_2 fluctuates less with depth, and on the whole, there is an increasing trend with depth. Combined with the results of paleoclimate analysis in the study area, it is found that the terrestrial debris input during the deposition of the Taodonggou Group strata has the characteristics of first an increasing and then a decreasing trend.

4.5.6 Paleoproductivity

Paleoproductivity determines the quantity of original organic matter in sedimentary rocks (Wei et al., 2012; Algeo and Ingall, 2007; Ross and Bustin, 2009; Schoepfer et al., 2015). The elements P, Si, Ba, Zn, and Cu are indicators of the magnitude of paleoproductivity, but they all have a certain range of application; for example, only the biogenic parts of Si and Ba can represent productivity, and Zn can only represent productivity change in the sulfide reduction environment (Wei et al., 2012; Algeo and Ingall, 2007).

P is not only a key nutrient element in biological metabolism but also an important component of many organisms, so it can also be used to characterize biological productivity (Kidder and Erwin, 2001). P /Ti and P / Al are commonly used to reflect biological productivity in order to eliminate the influence of terrigenous detritus. The P /Ti of Taodonggou Group mudstone in the study area ranges from $0.04\,\%$–$0.74\,\%$, with an average value of $0.17\,\%$ and an overall low productivity. As shown in Table A2, the relationship between P /Ti and depth was analyzed, and the results showed that the paleontological productivity tended to increase and then decrease with depth.

In addition, Cu is also an important nutrient and, unlike P, is generally indicative of productivity, including the sum of primary productivity and productivity from terrestrial inputs (Schoepfer et al., 2015). For the purpose of eliminating the dilution interference of terrigenous detritus, Cu / Ti is used as an indicator to evaluate the paleoproductivity in this study. The distribution range of Cu / Ti of Taodonggou Group mudstone in the study area is from 0.55 to 1.96, with an average

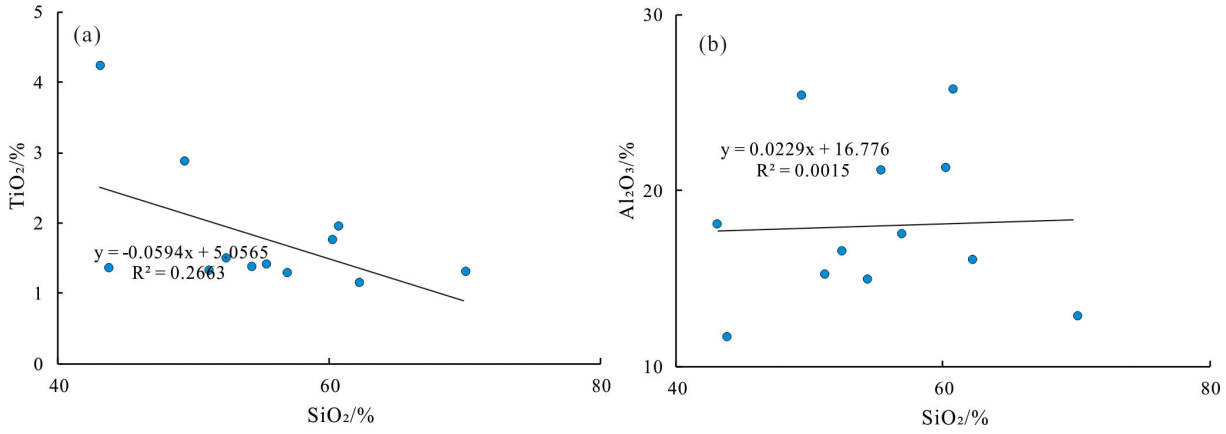

Figure 9. Intersection diagram of TiO_2 and SiO_2 **(a)** and intersection diagram of Al_2O_3 and SiO_2 **(b)**.

value of 1.02, and gradually decreases with depth, indicating a gradual increase in paleoproductivity during the deposition of Taodonggou Group mudstone.

4.5.7 Deposition rate

The deposition rate is one of the parameters characterizing the magnitude of the dilution effect during deposition and is commonly characterized by $(La / Yb)_N$. It is generally believed that the difference between LREE and HREE migration is not significant when the sedimentation rate of the lake basin is faster, and the $(La / Yb)_N$ value is close to 1. Conversely, when the $(La / Yb)_N$ value is greater or less than 1, it indicates that the sedimentation rate of the lake basin is slower (A. Wang et al., 2021; Cao et al., 2018). The $(La / Yb)_N$ values of the Taodonggou Group mudstones are 6.228–10.081, with an average value of 7.358 in the study area, which is much greater than 1. This indicates that the mudstone of the Taodonggou Group has a slower deposition rate.

4.5.8 Hydrothermal activity

The study area has been extremely volcanically active from the Carboniferous to the Permian, with extensive volcanic deposits in the middle Permian Taodonggou Group, the lower Permian Yierxitu Formation, and the Carboniferous. In order to explore whether hydrothermal activity is involved in the middle Permian sedimentation, the Zn–Ni–Co ternary diagram and the $(Cu + Co + Ni) \times 10$–Fe–Mn ternary diagram are applied in this study (Xu et al., 2022; You et al., 2019). Based on the Zn–Ni–Co ternary diagram (Fig. 10a), some data points of the Taodonggou Group mudstone are distributed in the hydrothermal sedimentary zone, and based on the $(Cu + Co + Ni) \times 10$–Fe–Mn ternary diagram (Fig. 10b), all data points of the samples fall in the hydrothermal sediment zone and Red Sea hydrothermal sediment zone, which indicates that the Taodonggou Group mudstone deposition was influenced by hydrothermal fluids.

4.5.9 Tectonic setting

Sedimentary rocks of different tectonic settings have prominent differences in element composition and content, so the geochemical characteristics of sedimentary rocks can be used to reflect the tectonic setting of sedimentary basins (Kroonenberg, 1992).

The elements Co, Th, Sc, Zr, and La are relatively stable and less affected by geological activities such as weathering, transportation, and deposition. Therefore, the La–Th–Sc ternary diagram and the Th–Co–Zr/10 ternary diagram can be utilized to distinguish the tectonic setting during the formation of sediments (Bhatia and Crook, 1986; Cai et al., 2022). Based on the La–Th–Sc ternary diagram (Fig. 11a), most of the data points fall in the continental island arc region, and based on the Th–Co–Zr/10 ternary diagram (Fig. 11b), almost all the data points fall in the continental island arc and oceanic island arc regions. This indicates that the tectonic setting of the Taodonggou Group's source area is a continental island arc and an oceanic island arc.

Additionally, previous studies have shown that SiO_2, TiO_2, Al_2O_3 / SiO_2, and $Fe_2O_3 + MgO$ are also important parameters for identifying the source tectonic setting. Cross-plots of Al_2O_3 / SiO_2 and $Fe_2O_3 + MgO$, TiO_2 and $Fe_2O_3 + MgO$, and SiO_2 and Al_2O_3 / SiO_2 are often employed to recognize the tectonic setting (Bhatia, 1983; Li et al., 2020; Roser and Korsch, 1988). Based on the cross-plot of Al_2O_3 / SiO_2 and $Fe_2O_3 + MgO$ (Fig. 11c), all data points are distributed around the continental island arc and oceanic island arc, which is consistent with the cross-plot of TiO_2 and $Fe_2O_3 + MgO$ (Fig. 11d) and the cross-plot of SiO_2 and Al_2O_3 / SiO_2 (Fig. 11e). As a result, the tectonic setting of the Taodonggou Group mudstone source area is continental island arc and oceanic island arc.

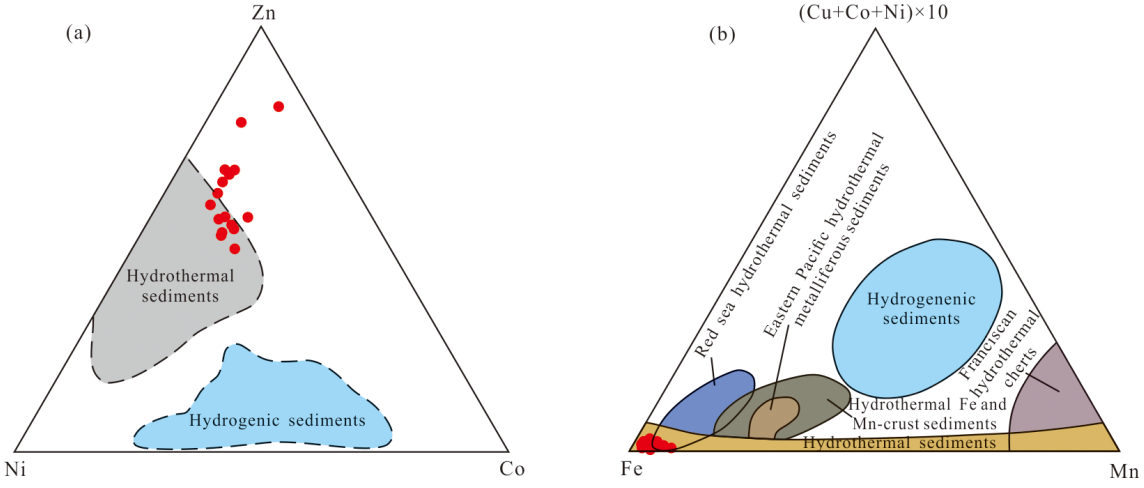

Figure 10. Zn–Ni–Co ternary diagram **(a)** and (Cu + Co + Ni) × 10–Fe–Mn ternary diagram **(b)** (modified after You et al., 2019).

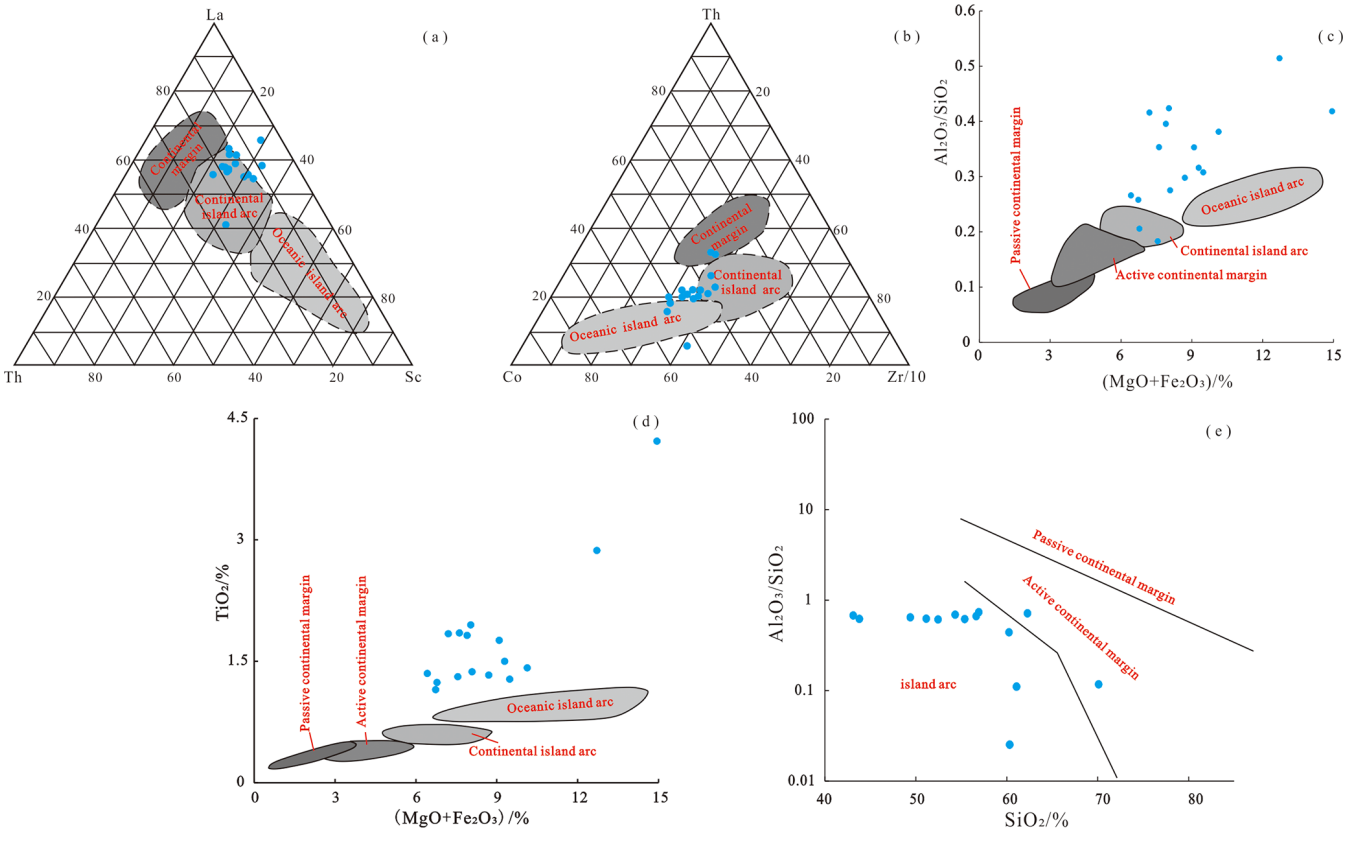

Figure 11. Tectonic setting of source area in Taodonggou Group mudstone: **(a)** La–Th–Sc ternary diagram (modified after Zhu et al., 2021), **(b)** Th–Co–Zr/10 ternary diagram (modified after Zhu et al., 2021), **(c)** cross-plot of Al_2O_3 / SiO_2 and Fe_2O_3+ MgO (modified after Bhatia, 1983), **(d)** cross-plot of TiO_2 and Fe_2O_3+ MgO (modified after Bhatia, 1983), **(e)** cross-plot of SiO_2 and Al_2O_3 / SiO_2 (modified after Roser and Korsch, 1988).

5 Discussion

The sedimentary environment, provenance location, and sedimentation mode are factors that influence the quality of mudstones. In this study, based on the mineralogical and elemental geochemical characteristics of the Taodonggou Group mudstones, we discuss the influence of sedimentary environment, provenance location, and sedimentation mode on the quality of the Taodonggou Group mudstones.

5.1 The influence of paleosedimentary environment on the quality of mudstone

Based on the mineralogical and elemental geochemical characteristics and previous studies on the organic geochemical characteristics of the Taodonggou Group mudstones (Miao et al., 2021), a comprehensive geochemical profile of well YT1 was established. The results are shown in Fig. 12. It can be observed from Fig. 12 that the sedimentary environment of the Taodonggou Group mudstones is closely related to their organic matter types and can be divided into three periods. In the early stage of the Taodonggou Group, the overall climate was warm and humid under moderate chemical-weathering conditions. The sedimentary waterbody was dysoxic–anoxic brackish water. At this time, productivity was weak, and organic matter was mainly derived from terrestrial sources. In the middle stage of the Taodonggou Group, the paleoclimate gradually shifted to a dry and humid climate under strong chemical-weathering conditions, accompanied by hydrothermal activity. This provided abundant nutrients for the growth of algae and other microorganisms. At the same time, the sedimentation rate increased, resulting in a predominance of algae in the organic matter composition during this period. During the late stage of the Taodonggou Group, the climate again shifted to a warm and humid climate under moderate chemical-weathering conditions. The sedimentation rate slowed down, and the input of organic matter shifted back to predominantly terrestrial sources.

5.2 Provenance

5.2.1 Lithology of parent rock

Previous studies have found that the chemical composition of the rocks in the sedimentary area and the parent rock in the provenance area have a strong affinity, and the type of parent rock will directly affect the elemental geochemical characteristics of the sediment (Tribovillard et al., 2006; Shi et al., 2021; McLennan et al., 1993; Basu et al., 2016; Hu et al., 2021; Floyd and Leveridge, 1987; Wronkiewicz and Condie, 1987). Generally speaking, the transport of sediment from the source area to the sedimentary area goes through multiple complex processes such as mechanical transport and chemical action, and hence it is necessary to analyze the impact of sediment sorting and recycling on each chemical component when identifying the source. Previous studies have shown that trace elements Zr, Th, and Sc are relatively stable in geological processes such as weathering, transportation, and sorting and are not easily lost, which can be used as one of the indicators for parent rock identification (Floyd and Leveridge, 1987; Wronkiewicz and Condie, 1987). According to the Th / Sc and Zr / Sc intersection diagram of Taodonggou Group mudstone (Fig. 13a), Taodonggou Group mudstone is close to andesite and felsic volcanic rock of the upper crust, and its composition is controlled by the composition of its felsic parent rock and has not undergone sediment sorting and recycling.

In addition, REE and trace elements in mudstone from different parent rocks are obviously different, so the ratio of REE to trace elements can be used to analyze the type of parent rock, and the most common ones are La / Sc, La / Co, Th / Sc, Th / Co, and Cr / Th (Basu et al., 2016; Hu et al., 2021; Floyd and Leveridge, 1987; Wronkiewicz and Condie, 1987; Allègre and Minster, 1978). Based on the Hf and La / Th intersection diagrams (Fig. 13b) and the La / Sc and Co / Th intersection diagrams (Fig. 13c), we can see that the mudstones of the Taodonggou Group have both andesitic island arc sources and felsic volcanic sources. It can be seen from the cross-plot of TiO_2 and Zr (Fig. 13d) that the mudstone of the Taodonggou Group is a source of intermediate igneous rocks and felsic igneous rocks. As can be seen from the cross-plot of La / Yb and Σ REE (Fig. 13e), almost all data points are located in the sedimentary rock, alkali basalt, and granite areas.

In summary, the parent rocks of the Taodonggou Group mudstone are andesitic and feldspathic volcanic rocks with weak sedimentary sorting and recirculation, and the material source information is well preserved.

5.2.2 Location of parent rock

There is a great deal of controversy about the provenance location of the middle Permian in the Turpan–Hami Basin (Shao et al., 2001; Jiang et al., 2015; J. L. Wang et al., 2019; Zhao et al., 2020; Song et al., 2018; Wang et al., 2018a, b; Tang et al., 2014). Shao et al. (1999) believed that the provenance of the Permian was mainly from the Jueluotage Mountains in the south of the Turpan–Hami Basin, Song et al. (2018) considered that it came from the Bogda area, and Zhao et al. (2020) believed that the provenance of the Permian in the Turpan–Hami Basin was consistent with that in the Junggar Basin and originated from the Kelameili mountains and the northern Tianshan. Summarizing the previous research results, it is found that the main controversial point is the time of the first uplift of the Bogda Mountains.

At present, there are many opinions about the time of the Bogda Mountain uplift, suggesting that it initially occurred in the early Permian (Carroll et al., 1990, 1995; Shu et al., 2011; Wang et al., 2018a; Li et al., 2022), middle Permian (Zhang et al., 2006; Liu et al., 2018; Wang et al., 2018b), late Permian–Early Triassic (Zhao et al., 2020; Guo et al.,

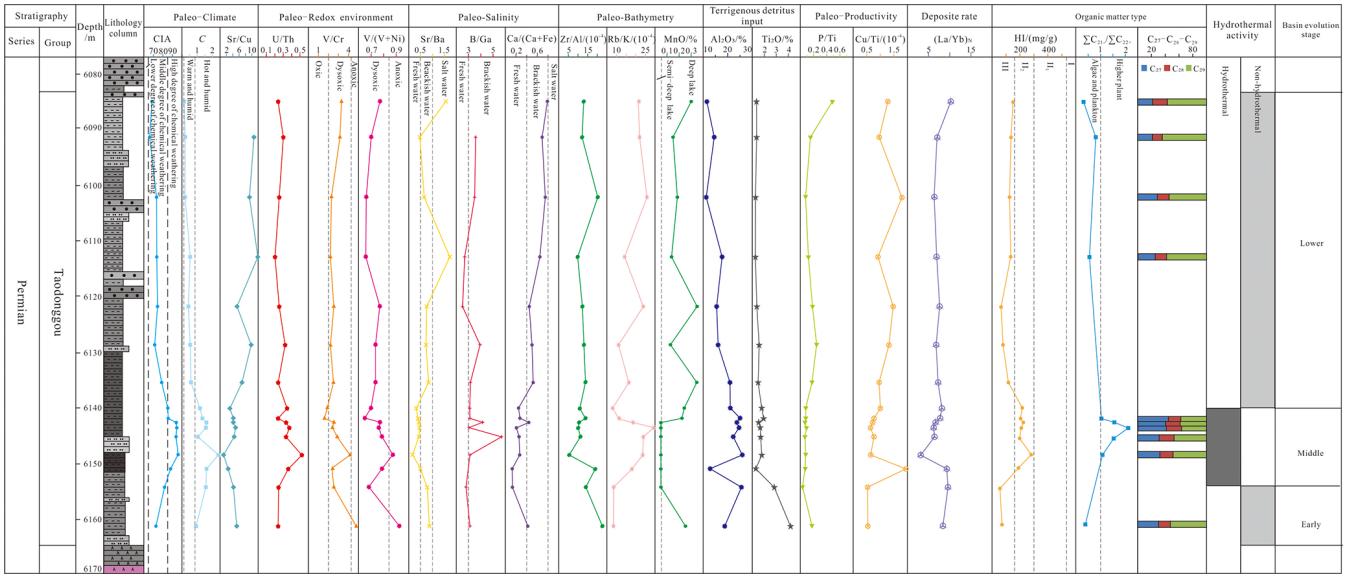

Figure 12. The geochemical profile of the Taodonggou Group in well YT1.

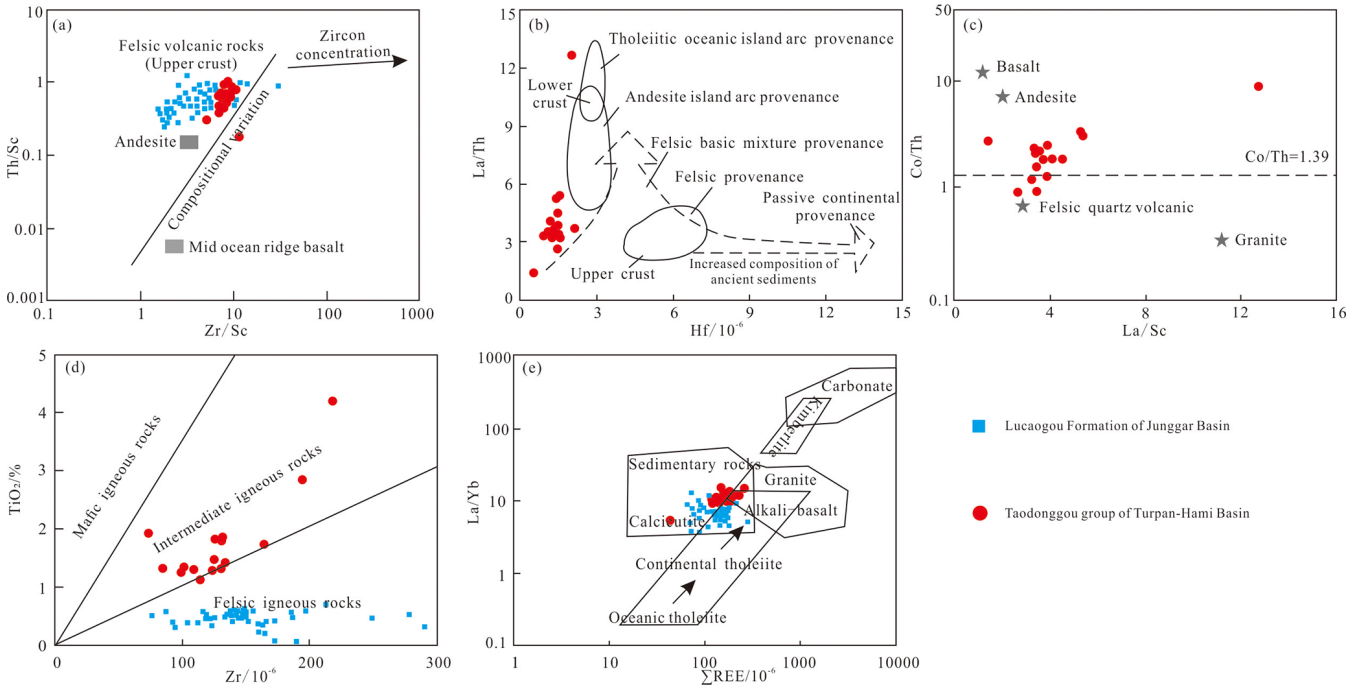

Figure 13. Parent rock type of the Taodonggou Group in well YT1 (data of Lucaogou Formation in the Junggar Basin are from Li et al., 2020): **(a)** Th / Sc and Zr / Sc intersection diagram (modified after Floyd and Leveridge, 1987), **(b)** La / Th and Hf intersection diagram (modified after Floyd and Leveridge, 1987), **(c)** Co / Th and La / Sc intersection diagram (modified after Wronkiewicz and Condie, 1987), **(d)** TiO_2 and Zr intersection diagram, **(e)** La / Yb and $\sum$ REE intersection diagram (modified after Allègre and Minster, 1978).

2006; Wang, 1996; Sun and Liu, 2009; Tang et al., 2014; Wang et al., 2018b), Middle Triassic (Guo et al., 2006), Early Jurassic (Green et al., 2005; Liu et al., 2017; Ji et al., 2018), and Late Jurassic (Yang et al., 2015). If the initial uplift of the Bogda Mountains was after the middle Permian, the parent rock types of the Taodonggou Group mudstone in the Turpan–Hami Basin and the Lucaogou Formation mudstone in the Junggar Basin should be the same.

We have counted the elemental geochemical characteristics of the Lucaogou Formation in the Junggar Basin (Li et al., 2020) and found that the parent rock type of Lucaogou Formation mudstone in the Junggar Basin is greatly different

from that of P_2td, which is felsic volcanic rock (Fig. 14). As a result, the Bogda Mountains' initial uplift should be late Permian–Early Triassic in the early Permian or middle Permian. This is consistent with Li et al. (2022) and Wang et al. (2018a), who inferred the uplift of the Bogda Mountains at 289.8–265.7 Ma. Shao et al. (2001) believed that the sandstone of the Daheyan Formation in the Turpan–Hami Basin has a good affinity with the early Permian and Carboniferous, so the provenance direction of the sandstone of the Daheyan Formation is consistent with that of the early Permian, and they all come from the Jueluotage Mountains. However, the paleocurrent direction of the early Permian in Xinjiang is southeast (Zhang et al., 2005; Li et al., 2007; J. L. Wang et al., 2019), and the provenance area is located in the north of the Bogda area. Zhao et al. (2020) calculated the U–Pb dating results of 5250 zircons in the Tianshan and believed that the provenances of the Turpan–Hami Basin and the Junggar Basin both came from the northern Tianshan and the Kelameili mountains, which is also consistent with the ancient ocean current direction in the early Permian (Zhang et al., 2005; Li et al., 2007; J. L. Wang et al., 2019; Fig. 14a). Consequently, the first uplift of the Bogda Mountains should have occurred in the early Permian, but it was not exposed in the early–middle Permian, and it still received sedimentation. In the middle Permian, the exposed water began to be denuded, becoming the source area of the Turpan–Hami Basin (Wang et al., 2018a).

Based on the above analysis, in the early–middle Permian, although the Bogda Mountains in the north of the Turpan–Hami Basin were uplifted due to orogeny, it did not emerge from the water surface, and it still accepted the provenance of the northern Tianshan and Kelameili mountains. At this time, there was a NE-trending ancient ocean current (Carroll et al., 1995; Obrist-Farnert et al., 2015; Zhao et al., 2020), so the Jueluotage Mountains, which had been uplifted in the south of the Turpan–Hami Basin, became a secondary provenance area (Shao et al., 1999; Fig. 14b). With the continuous uplift of the Bogda Mountains, the sedimentary center of the Turpan–Hami Basin gradually shifted to Taibei Sag, and the provenance area of the Turpan–Hami Basin changed to the Bogda and Jueluotage mountains (Fig. 14c).

5.3 Sedimentation mode

In previous studies, scholars have believed that the sedimentation of the Permian in the Turpan–Hami Basin is mainly controlled by traction currents (Chen et al., 2003). However, recent research has revealed the presence of gravity flow deposits in the Permian of the Turpan–Hami Basin (2018a; Xu, 2022). Yang et al. (2010) found poorly sorted debris flow deposits in the Daheyan Formation, and Xu (2022) discovered alluvial and fluvial facies in the Daheyan Formation, consisting of volcaniclastic rocks and conglomerates that are similar in composition to the lower Permian volcaniclastic rocks and conglomerates. This suggests the existence of gravity flow deposits during the early Permian in the Turpan–Hami Basin. Wang et al. (2018a) also suggested the development of gravity flow deposits and pillow lavas in the early Permian. Meanwhile, in the early–middle Permian, the sedimentation inherited the provenance and sedimentation style from the early Permian, but the gravity flow deposits transitioned gradually into traction current deposits. Due to the influence of gravity flow deposits, terrestrial organic matter can be transported to the deep lake area (Yu et al., 2022; Li et al., 2011), thereby altering the type of organic matter.

During the middle of the Taodonggou Group, the Turpan–Hami Basin entered the foreland basin sedimentation stage due to the uplift of the Bogda Mountains. The sedimentary environment of the Taodonggou Group in the Tainan Sag is similar to that in the Taibei Sag (Li, 2019). During this time, the sedimentary waterbody of the Taodonggou Group in the Turpan–Hami Basin became shallower, and the dominant sedimentation style transitioned to traction currents. Xu (2022) conducted lithological observations on the Taerlanggou section, the Zhaobishan section, and the well YT1 in the Taodonggou Group and found the presence of traction structures of gravity flow origin in the middle and upper parts of the Taerlang Formation. Additionally, a large number of calcareous and iron nodules appeared in the formation, indicating the occurrence of gravity flow deposits during the late-stage sedimentation of the Taodonggou Group. The organic matter type in the mudstones during this period was influenced by gravity flows.

5.4 Formation mechanism of the Taodonggou Group mudstone

Based on the sedimentary environment, provenance, and sedimentation mode during the deposition of the Taodonggou Group mudstones, this study has constructed the formation mechanism of the Taodonggou mudstones. The results indicate that the formation of the Taodonggou Group mudstones can be divided into three stages.

In the early part of the Taodonggou Group, the Bogda Mountains began to rise but did not emerge from the water surface. The sediment source is mainly from the northern Tianshan and Kelameili mountains, and the secondary source area is the Jueluotage Mountains in the south of the Turpan–Hami Basin. The stratum of the Taodonggou Group was deposited in a warm and humid paleoclimate with high weathering intensity and a stable input of terrigenous detritus. In addition, the sedimentary waterbody is deep at this time, creating a deep lake environment of brackish and dysoxic water. However, this period inherited the gravity flow sedimentation characteristics from the early Permian. Due to the influence of gravity flows, terrestrial organic matter was transported to the deep lake, resulting in the input of organic matter in the mudstones primarily derived from higher terrestrial plants (Miao et al., 2021). Consequently, a high-quality Type III organic matter source rock was formed (Fig. 15a).

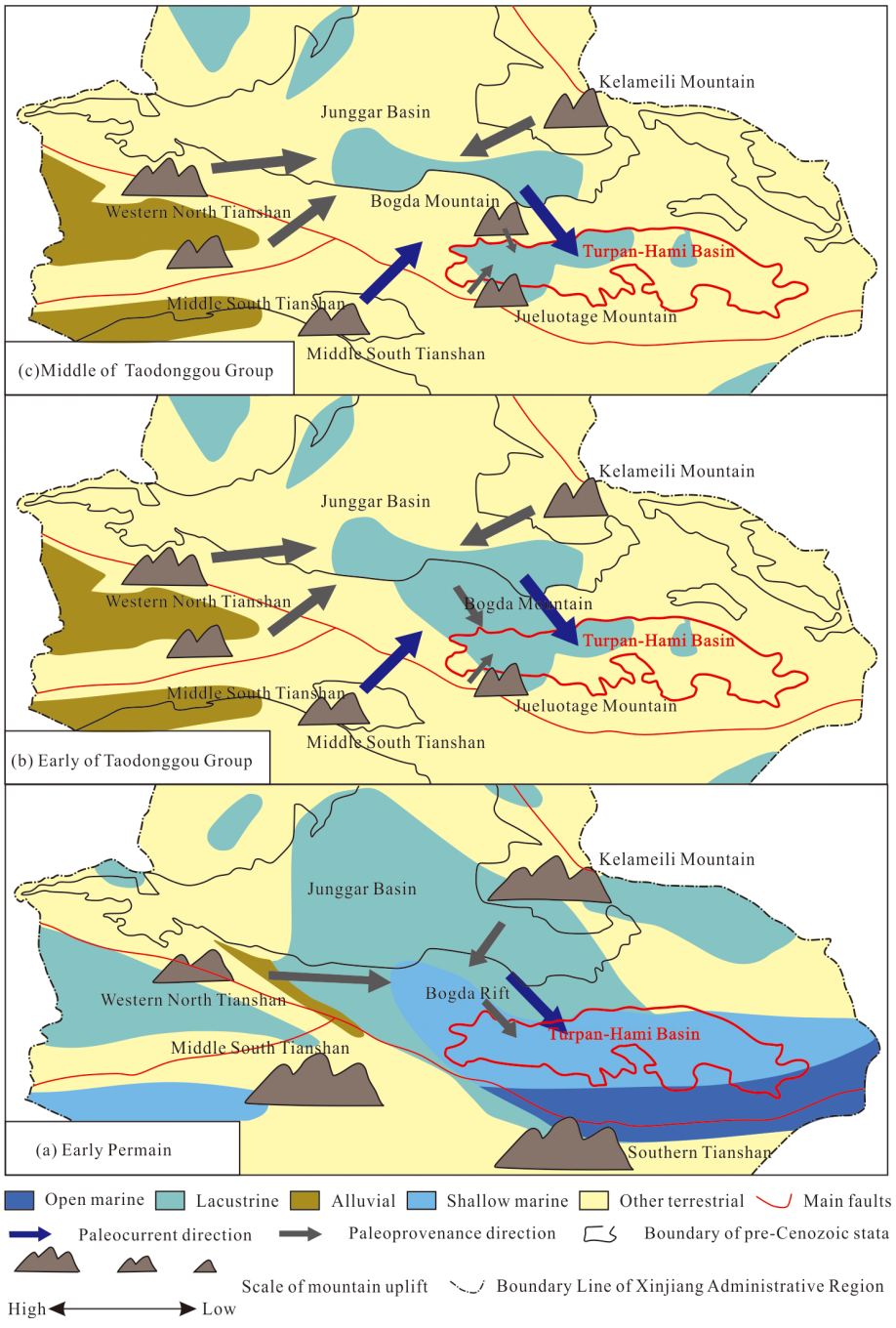

Figure 14. Provenance location from early Permian to middle Permian in the Tianshan area (modified after Zhao et al., 2020): **(a)** early Permian, **(b)** early Taodonggou Group, **(c)** middle to later Taodonggou Group.

In the middle of the Taodonggou Group, with the continuous uplift of the Bogda Mountains and hydrothermal activity, the climate changed into a hot and humid paleoclimate, the weathering degree further increased, and the input of terrigenous detritus increased. The provenance areas are the Bogda and Jueluotage mountains. In addition, during this period, the sedimentary center gradually transferred to the Taibei Sag, and the sedimentary waterbody became shallow, which was a dysoxic, intermediate-depth lake environment. Due to the nutrients brought by hydrothermal activity, the lower algae multiplied during this period, and the salinity of the sedimentary water body became lower, becoming a freshwater environment and thus depositing a set of high-quality Type II_2 organic source rocks.

In the late Taodonggou Group, the uplift of the Bogda Mountains basically stopped, and the climate changed to a

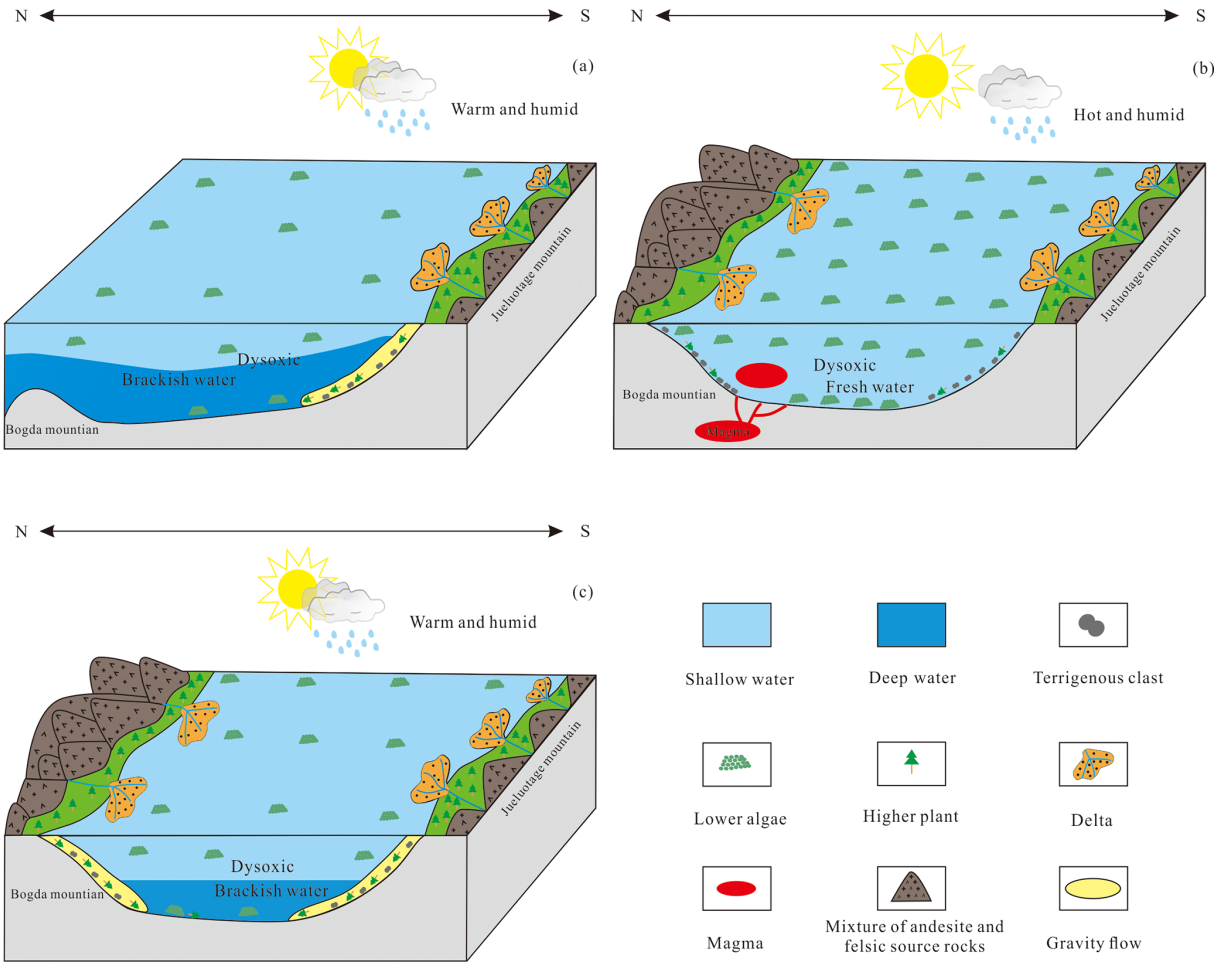

Figure 15. Middle Permian source–sink system and lake basin evolution history of the Turpan–Hami Basin: **(a)** early Taodonggou Group, **(b)** middle Taodonggou Group, **(c)** late Taodonggou Group.

warm and humid paleoclimate again. The weathering degree was high, and the input of terrigenous debris was reduced. The Bogda and Jueluotage mountains remained the provenance areas. The sedimentary center was essentially transferred to the Taibei Sag at this time. During this period, the salinity of the sedimentary waterbody was high, and the sedimentary waterbody became deeper. It was a deep lake environment with dysoxic and brackish water. During this period, the sedimentation was also influenced by gravity flows, leading to changes in lithology and organic matter type. As a result, the organic matter type in the mudstones deposited during this period transitioned to Type III.

6 Conclusions

Through the mineral composition and element geochemistry analysis of the Taodonggou Group mudstone, the following insights have been obtained:

1. The mudstone minerals of the Taodonggou Group are mainly clay and quartz and can be classified into four petrographic types according to their mineral fractions.

2. The Taodonggou Group mudstone was deposited in an intermediate-depth or deep, dysoxic, freshwater–brackish lake environment under warm and humid paleoclimatic conditions. The input of terrestrial debris was stable, but the sedimentation rate was slow. In addition, the sedimentation in the middle stage was influenced by hydrothermal activities. Moreover, the source rocks of the Taodonggou Group mudstone are mainly andesitic and feldspathic volcanic rocks. Sediment sorting and recycling were weak, and hydrocarbon source information was well preserved. The tectonic background of the source area was a continental island arc and an oceanic island arc.

3. The sedimentary environment, sources, and sedimentary methods have significant impacts on the organic matter types of the Taodonggou Group. In the early

Taodonggou Group, the sedimentation center was in the Bogda area. At this time, the Bogda Mountain region was not exposed, and the depositional processes inherited the characteristics of early Permian gravity flow sedimentation, resulting in the widespread deposition of a series of high-quality Type III source rocks in the basin. In the middle Taodonggou Group, the sedimentation center gradually migrated to the Taibei Sag. During this period, the Bogda Mountain region experienced uplift and hydrothermal activity, and the depositional processes gradually transitioned to traction flows, resulting in the widespread deposition of a series of Type II source rocks in the basin. In the late Taodonggou Group, the uplift of the Bogda Mountain region ceased, and the sedimentation center completely shifted to the Taibei Sag. Meanwhile, under the influence of gravity flows, the organic matter types of the Taodonggou mudstone changed to Type III.

Appendix A

Table A1. Mineral composition of Taodonggou Group mudstone in well YT1.

Samples	Depth (m^{-1})	Mineral content ($\%^{-1}$)							
		Quartz	*K*-feldspar	Plagioclase	Calcite	Siderite	Pyrite	Baryte	Clay
YT1-1	6084	29.4	0.7	1.8	23.7	/	/	13.3	31.1
YT1-2	6092	30.1	1.1	5.4	26.9	/	/	2.1	34.4
YT1-3	6102	41.9	/	2.5	18.1	/	/	3.2	34.3
YT1-4	6113	35.7	0.5	2.9	10.8	/	/	2.8	47.3
YT1-5	6122	40.5	0.1	2.7	19.4	/	/	4.6	32.7
YT1-6	6129	39.2	0.6	2.1	19.7	/	/	4	34.4
YT1-7	6136	27.9	0.3	0.8	42.8	/	/	4.3	23.9
YT1-8	6140	31.2	0.6	0.6	22.1	/	/	5.6	39.9
YT1-9	6143	34	0.4	0.2	14	/	/	4.5	46.9
YT1-10	6144.7	33.6	2.1	3.7	11.4	2.1	2.8	3.5	40.8
YT1-11	6145.3	37	/	3.7	10.6	1.4	/	2.1	45.2
YT1-12	6145.8	38.4	1.7	2.2	12.5	/	/	3.1	42.1
YT1-13	6147	37.9	/	/	1	/	1.4	1.2	58.5
YT1-14	6151	59.2	0.5	0.2	1.3	/	2.1	/	36.7
YT1-15	6154	21.8	0.8	0.8	1.8	/	/	3.9	70.9
YT1-16	6161	17.2	2.3	4.8	35.4	2	/	5	33.3

Table A2. Major elements of Taodonggou Group mudstone in well YT1.

Samples	Depth (m^{-1})	Content ($\%^{-1}$)										CIA	P /Ti	K_2O / Al_2O_3
		SiO_2	CaO	Al_2O_3	Fe_2O_3	K_2O	TiO_2	Na_2O	MgO	P_2O_5	MnO			
YT1-1	6084	43.79	19.05	11.65	5.32	3	1.35	1.15	1.1	0.9	0.3	68.71	0.49	0.26
YT1-2	6092	54.32	14.01	14.96	6.74	3.39	1.37	1.5	1.34	0.29	0.15	70.1	0.15	0.23
YT1-3	6102	56.63	14.36	11.66	5.42	3.38	1.24	1.23	1.36	0.16	0.19	66.63	0.09	0.29
YT1-4	6113	56.92	7.38	17.52	7.93	4.2	1.28	1.22	1.55	0.21	0.14	72.55	0.12	0.24
YT1-5	6122	51.15	12.62	15.25	7.55	3	1.33	1.2	1.15	0.3	0.34	73.85	0.17	0.20
YT1-6	6129	62.28	4.49	16.07	5.93	3.5	1.15	1.68	0.8	1.17	0.12	70.08	0.74	0.22
YT1-7	6136	52.44	9.31	16.57	8.63	2.54	1.5	1.55	0.66	0.37	0.34	74.57	0.18	0.15
YT1-8	6140	55.37	3.01	21.11	9.64	2.63	1.42	1.5	0.49	0.15	0.24	78.92	0.08	0.12
YT1-9	6143	60.24	2.76	21.27	8.73	1.92	1.76	0.84	0.36	0.23	0.22	85.5	0.09	0.09
YT1-10	6144.7	61.08	2.75	24.16	7.54	0.99	1.82	0.3	0.36	0.21	0.06	93.83	0.08	0.04
YT1-11	6145.3	61.02	2.94	25.39	6.84	0.59	1.84	0.31	0.36	0.26	0.06	95.45	0.10	0.02
YT1-12	6145.8	60.32	5.41	21.32	7.29	0.72	1.85	0.34	0.32	0.21	0.06	93.84	0.08	0.03
YT1-13	6147	60.76	1.83	25.75	7.68	0.68	1.95	0.19	0.35	0.25	0.05	96.07	0.09	0.03
YT1-14	6151	70.11	2.44	12.83	7.28	0.97	1.31	0.34	0.27	0.15	0.05	88.59	0.09	0.08
YT1-15	6154	49.39	1.92	25.41	12.25	2.84	2.87	1.57	0.46	0.15	0.06	80.97	0.04	0.11
YT1-16	6161	43.11	9.56	18.04	14.17	2.83	4.22	1.9	0.77	1.03	0.25	73.12	0.18	0.16

Table A3. Characteristics of trace elements in Taodonggou Group mudstone.

Samples		YT1-1	YT1-2	YT1-3	YT1-4	YT1-5	YT1-6	YT1-7	YT1-8	YT1-9	YT1-10	YT1-11	YT1-12	YT1-13	YT1-14	YT1-15	YT1-16
Depth (m^{-1})		6084	6092	6102	6113	6122	6129	6136	6140	6143	6144.7	6145.3	6145.8	6147	6151	6154	6161
Content (ppm^{-1})	Be	0.952	1.12	1.67	1	1.52	1.26	1.74	2.17	1.79	1.31	1.35	1.42	0.711	1.77	2.05	1.55
	Sc	9.02	11.9	15.5	11.7	13.6	13.1	15.6	16.2	21.2	11.4	13.2	12.3	7	24	26	17.6
	V	87.3	64.2	72	59.5	106	89.2	100	88.5	88.7	122.3	114.6	131.6	177	145	124	199
	Cr	27.4	21.2	31.8	27.3	40.1	43	40.1	45.1	54.8	48.5	47.6	44.5	43	63	51	40.2
	Co	9.46	12.4	14.9	13.3	11.9	12.6	13.7	18.2	27.6	22.3	21.7	20.6	18.7	24.8	36.9	30.4
	Ni	25.5	27.8	36.7	32.5	32.6	33.2	37.8	37.2	47.5	36.8	35.7	34.6	27.3	41.7	55.4	17.9
	Cu	34.2	33.1	44.8	34.6	51.2	41.8	39.9	50.8	48.9	52.6	50.3	51.4	57.3	55.8	64.4	71.2
	Zn	125	79	92.4	96.1	69.8	90.4	74.4	67.9	78.7	64.6	63.2	65.8	44.1	70.4	114	218
	Ga	17.81	20.1	23.3	19	24.8	21.9	15.1	13.2	16.1	14.5	12.7	13.7	7.14	12.7	19.2	17.3
	Rb	54.5	64.6	73.5	50.4	60	33.5	33.9	16	17.9	15.6	14.6	14.6	13.6	14.2	21	20.7
	Sr	758	357	420	422	291	414	269	151	199	214	244	224	63.9	126	263	393
	Mo	1.29	0.661	0.866	1.24	1.09	1.44	1.17	1.23	2.68	3.02	2.88	3.14	3.86	2.14	1.18	1.28
	Ba	483.83	735.7	633	547.28	159.24	547.66	326.49	465.2	565	503	516	505	427	254	303.56	424.35
	B	46.31	71.3	81.4	67.4	64.5	55.4	60.2	41.3	49.6	44.6	52.6	41.4	41.5	39.7	56.2	54.1
	Th	9.16	6.03	7.31	6.43	8.38	12.4	10.3	10.4	10	9.12	8.33	8.86	6.17	7.32	9.96	3.13
	U	2.13	1.8	1.83	2.14	1.66	3.1	3.17	2.43	2.06	3.1	3.06	2.89	3.2	2.66	2.42	0.73
	Zr	82.7	99.3	124	97.1	107	112	123	132	162	128.8	130.2	123.6	70.8	130.4	192	215
	Hf	2.6	3.77	4.29	3.51	3.87	4.03	4.45	4.76	5.52	4.76	3.94	4.01	2.23	3.21	6.13	6.29
Sr / Ba		1.57	0.49	0.66	0.77	1.83	0.76	0.82	0.32	0.35	0.43	0.47	0.44	0.15	0.5	0.87	0.93
Ga / Rb		0.33	0.31	0.32	0.38	0.41	0.65	0.45	0.83	0.9	0.93	0.87	0.94	0.53	0.89	0.91	0.84
B / Ga		2.6	3.55	3.49	3.55	2.6	2.53	3.99	3.13	3.08	3.08	4.14	3.02	5.81	3.13	2.93	3.13
Rb / K/(10^{-4})		21.87	22.94	26.18	14.45	24.08	11.52	16.07	7.32	11.22	18.97	29.79	24.41	24.08	17.63	8.9	8.81
V / Cr		3.19	3.03	2.26	2.18	2.64	2.07	2.49	1.96	1.62	2.52	2.41	2.96	4.12	2.3	2.43	4.95
V / (V + Ni)		0.77	0.7	0.66	0.65	0.76	0.73	0.73	0.7	0.65	0.77	0.76	0.79	0.87	0.78	0.69	0.92
C		0.22	0.32	0.26	0.54	0.43	0.53	0.61	1.19	1.38	1.61	1.56	1.03	2.42	1.64	1.56	0.93

Table A4. Enrichment factors of the Taodonggou Group mudstone after AS transformation.

Samples	X_{EF}																	
	Be	Sc	V	Cr	Co	Ni	Cu	Zn	Ga	Rb	Sr	Mo	Ba	B	Th	U	Zr	Hf
YT1-1	0.43	0.11	0.92	0.42	0.68	0.51	1.04	1.80	1.28	0.53	3.66	0.63	1.14	0.68	1.05	0.78	0.71	1.28
YT1-2	0.39	0.12	0.53	0.25	0.70	0.44	0.78	0.89	1.13	0.49	1.34	0.25	1.35	0.82	0.54	0.52	0.66	1.44
YT1-3	0.75	0.19	0.76	0.48	1.07	0.74	1.36	1.33	1.68	0.72	2.03	0.43	1.49	1.20	0.83	0.67	1.06	2.11
YT1-4	0.30	0.10	0.42	0.28	0.64	0.43	0.70	0.92	0.91	0.33	1.36	0.41	0.86	0.66	0.49	0.52	0.55	1.15
YT1-5	0.52	0.13	0.85	0.47	0.66	0.50	1.19	0.77	1.37	0.45	1.07	0.41	0.29	0.73	0.73	0.47	0.70	1.45
YT1-6	0.41	0.12	0.68	0.47	0.66	0.48	0.92	0.94	1.14	0.24	1.45	0.51	0.94	0.59	1.03	0.83	0.69	1.44
YT1-7	0.55	0.14	0.74	0.43	0.69	0.53	0.85	0.75	0.77	0.23	0.91	0.40	0.54	0.62	0.83	0.82	0.74	1.54
YT1-8	0.54	0.11	0.51	0.38	0.72	0.41	0.85	0.54	0.52	0.09	0.40	0.33	0.61	0.34	0.66	0.49	0.62	1.29
YT1-9	0.44	0.14	0.51	0.46	1.09	0.52	0.81	0.62	0.64	0.10	0.53	0.72	0.73	0.40	0.63	0.42	0.76	1.49
YT1-10	0.28	0.07	0.62	0.36	0.77	0.36	0.77	0.45	0.50	0.07	0.50	0.72	0.57	0.32	0.50	0.55	0.53	1.13
YT1-11	0.28	0.08	0.55	0.33	0.72	0.33	0.70	0.42	0.42	0.07	0.54	0.65	0.56	0.36	0.44	0.52	0.51	0.89
YT1-12	0.35	0.08	0.76	0.37	0.81	0.38	0.85	0.52	0.54	0.08	0.59	0.84	0.65	0.33	0.55	0.58	0.58	1.08
YT1-13	0.14	0.04	0.84	0.30	0.61	0.25	0.79	0.29	0.23	0.06	0.14	0.86	0.46	0.28	0.32	0.53	0.27	0.50
YT1-14	0.72	0.27	1.39	0.87	1.62	0.76	1.54	0.92	0.83	0.13	0.55	0.95	0.54	0.53	0.76	0.89	1.01	1.43
YT1-15	0.42	0.15	0.60	0.36	1.22	0.51	0.90	0.75	0.63	0.09	0.58	0.27	0.33	0.38	0.52	0.41	0.75	1.38
YT1-16	0.45	0.14	1.35	0.39	1.41	0.23	1.40	2.03	0.81	0.13	1.23	0.41	0.65	0.51	0.23	0.17	1.19	2.00
Average	0.41	0.12	0.73	0.40	0.87	0.44	0.93	0.79	0.75	0.20	0.91	0.56	0.68	0.50	0.59	0.55	0.68	1.29

Table A5. Characteristics of REE in Taodonggou Group mudstone.

Samples	Depth (m^{-1})	Content (ppm)																	$(La/Yb)_N$
		La	Ce	Pr	Nd	Sm	Eu	Gd	Tb	Dy	Ho	Er	Tm	Yb	Lu	∑REE	LREE	MREE	HREE	
YT1-1	6084	31.70	57.70	6.73	28.80	5.14	1.46	5.19	0.72	3.89	0.68	2.17	0.30	2.12	0.352	146.953	124.930	17.077	4.946	10.081
YT1-2	6092	27.30	47.80	5.51	22.90	4.79	0.84	4.13	0.73	4.25	0.71	2.40	0.37	2.56	0.408	124.695	103.510	15.447	5.738	7.190
YT1-3	6102	27.30	48.30	5.62	23.10	4.71	1.32	4.17	0.80	4.63	0.88	2.68	0.41	2.89	0.464	127.271	104.320	16.511	6.440	6.369
YT1-4	6113	26.40	45.60	5.20	22.20	4.37	0.96	4.09	0.68	3.88	0.72	2.35	0.36	2.56	0.408	119.783	99.400	14.705	5.678	6.953
YT1-5	6122.	32.60	62.80	7.61	31.70	6.56	1.96	5.77	0.98	5.35	0.97	2.89	0.43	2.92	0.429	162.971	134.710	21.590	6.671	7.527
YT1-6	6129	33.10	80.10	7.48	31.70	6.19	0.62	5.98	0.99	5.58	0.99	3.01	0.50	3.31	0.564	180.108	152.380	20.345	7.383	6.742
YT1-7	6136	33.50	66.40	7.70	31.20	6.19	1.18	5.46	0.91	5.24	0.96	3.05	0.49	3.18	0.454	165.914	138.800	19.936	7.178	7.102
YT1-8	6140	35.90	65.80	7.23	29.20	5.47	1.65	4.96	0.96	5.35	0.96	2.97	0.47	3.01	0.426	164.346	138.130	19.344	6.872	8.041
YT1-9	6143	39.00	73.40	9.60	40.00	7.18	1.44	5.64	1.02	5.91	1.08	3.45	0.52	3.41	0.519	192.169	162.000	22.270	7.899	7.711
YT1-10	6144.7	32.60	66.43	7.34	26.40	6.31	0.98	4.82	0.84	4.97	0.86	3.12	0.33	3.21	0.436	158.646	132.770	18.130	7.096	6.847
YT1-11	6145.3	27.90	62.23	5.23	23.20	5.42	1.04	4.46	0.92	5.41	0.88	2.88	0.44	3.02	0.423	143.453	118.560	17.880	6.763	6.228
YT1-12	6145.8	30.20	65.60	5.64	25.40	5.93	1.02	5.01	0.47	4.54	0.91	2.94	0.46	3.01	0.501	151.631	126.840	5.531	6.911	6.764
YT1-13	6147	8.84	16.80	1.75	6.90	1.39	0.30	1.32	0.27	1.87	0.39	1.27	0.22	1.67	0.265	43.247	34.290	5.531	3.426	3.569
YT1-14	6151	39.40	73.60	8.64	33.60	4.22	1.84	4.32	1.21	5.83	1.03	3.42	0.43	2.98	0.392	180.912	155.240	5.531	7.222	8.914
YT1-15	6154	52.60	105.00	12.30	50.80	9.09	2.45	7.65	1.25	7.14	1.16	3.86	0.57	3.62	0.510	257.997	220.700	28.740	8.557	9.796
YT1-16	6161	39.70	85.70	11.10	52.10	9.76	2.29	8.33	1.34	7.47	1.25	3.75	0.52	3.39	0.502	227.206	188.600	30.440	8.166	7.895

LREE = La + Ce + Pr + Nd. MREE = Sm + Eu + Gd + Tb + Dy + Ho. HREE = Er + Tm + Yb + Lu. $(La/Yb)_N = (La/Yb)/(La/Yb)_{chondrite}$.

Data availability. Data will be made available on request.

Author contributions. HM and JG designed the experiments; YW and ZJ revised the first draft of the manuscript; JG, YW, and ZJ procured funding; HM and CZ provided language services and figure production; and CL investigated and revised the ideas of the article. All authors contributed to the review of the manuscript.

Competing interests. The contact author has declared that none of the authors has any competing interests.

Disclaimer. Publisher's note: Copernicus Publications remains neutral with regard to jurisdictional claims in published maps and institutional affiliations.

Acknowledgements. This study was supported by the National Major Science and Technology Project of China (grant nos. 2016ZX05066001-002, 2017ZX05064-003-001, 2017ZX05035-02, and 2016ZX05034-001-05), the Innovative Research Group Project of the National Natural Science Foundation of China (grant nos. 41872135, 42072151, and 42372144), a PetroChina science and technology project (grant no. 2021DJ0602), and the National Energy Shale Gas R&D (Experiment) Center (grant no. 2022-KFKT-15). We thank Hangzhou Yanqu Information Co., Ltd, as well as the Key Laboratory of Natural Gas Accumulation, the Re-

search Institute of Petroleum Exploration and Development, and Beijing Orient Smart for providing testing samples and test equipment. We also thank our colleagues for their useful suggestions.

Financial support. This research has been supported by the National Major Science and Technology Projects of China (grant nos. 2016ZX05066001-002, 2016ZX05034-001-05, 2017ZX05064-003-001, and 2017ZX05035-02), the Innovative Research Group Project of the National Natural Science Foundation of China (grant nos. 41872135 and 42072151), the PetroChina Company Limited (grant no. 2021DJ0602), and the National Energy Shale Gas R&D (Experiment) Center (grant no. 2022-KFKT-15).

Review statement. This paper was edited by Andrea Di Muro and reviewed by three anonymous referees.

References

Algeo, T. J. and Ingall, E.: Sedimentary Corg:P ratios, paleocean ventilation, and Phanerozoic atmospheric pO_2, Palaeogeogr. Palaeocl., 256, 130–155, 2007.

Algeo, T. J. and Maynard, J. B.: Trace-element behavior and redox facies in core shales of Upper Pennsylvanian Kansas-type cyclothems, Chem. Geol., 206, 289–318, 2004.

Allègre, C. J. and Minster, J. F.: Quantitative models of trace element behavior in magmatic processes, Earth Planet. Sc. Lett., 38, 1–25, 1978.

Basu, A., Bickford, M. E., and Deasy, R.: Inferring tectonic provenance of siliciclastic rocks from their chemical compositions: A dissent, Sediment. Geol., 336, 26–35, 2016.

Bhatia, M. R.: Plate tectonics and geochemical composition of sandstones, J. Geol., 91, 611–627, 1983.

Bhatia, M. R. and Crook, K. A. W.: Trace element characteristics of graywackes and tectonic setting discrimination of sedimentary basin, Contrib. Mineral. Petrol., 92, 181–193, 1986.

Cai, Y. L., Ouyang, F., Luo, X. R., Zhang, Z. L., Wen, M. L., Luo, X. N., and Tang, R.: Geochemical Characteristics and Constraints on Provenance, Tectonic Setting, and Paleoweathering of Middle Jurassic Zhiluo Formation Sandstones in the Northwest Ordos Basin, North-Central China, Minerals, 12, 603, https://doi.org/10.3390/min12050603, 2022.

Cao, J., Yang, R. F., Yin, W., Hu, G., Bian, L. Z., and Fu, X. G.: Mechanism of Organic Matter Accumulation in Residual Bay Environments: The Early Cretaceous Qiangtang Basin, Tibet, Energ. Fuels, 32, 1024–1037, 2018.

Cao, L., Zhang, Z. H., Zhao, J. Z., Jin, X., Li, H., Li, J. Y., and Wei, X. D.: Discussion on the applicability of Th / U ratio for evaluating the paleoredox conditions of lacustrine basins, Int. J. Coal Geol., 248, 103868, https://doi.org/10.1016/j.coal.2021.103868, 2021.

Carroll, A., Liang, Y. H., Graham, S., Xiao, X. H., Hendrix, S., Chu, J. C., and McKnight, L.: Junggar basin, northwest China: trapped Late Paleozoic Ocean, Tectonophysics, 181, 1–14, 1990.

Carroll, A., Graham, S., Hendrix, M., Ying, D., and Zhou, D.: Late Paleozoic tectonic amalgamation of northwestern China: sedimentary record of the northern Tarim, northwestern Turpan, and southern Junggar basins, Geol. Soc. Am. Bull., 107, 571–594, 1995.

Chen. X., Niu, R. J., and Cheng, J. H.: The Sequence stratigraphy of Middle Permian-Triassic in Turpan-Hami Basin, Xinjiang, Pet. Geol., 24, 494–497, 2003.

Deditius, A.: Arsenic Environmental Geochemistry, Mineralogy, and Microbiology, Rev. Mineral. Geochem., 79, 1905–1907, 2015.

Essefi, E.: Geochemistry and mineralogy of the sebkha Oum El Khialate evaporites mixtures, southeastern Tunisia, Resour. Geol., 71, 242–249, 2021.

Floyd, P. A. and Leveridge, B. E.: Tectonic environment of the Devonian Gramscatho Basin, South cornwall: framework mode and geochemical evidence from turibiditic sandstones, J. Geol. Soc., 144, 531–542, 1987.

Gehrels, G. E., Valencia, V. A., and Ruiz, J.: Enhanced precision, accuracy,efficiency, and spatial resolution of U-Pb ages by laser ablation-multicollector-inductively coupled plasma-massspectrometry, Geochem. Geophy. Geosy., 9, 1–13, 2008.

Glaser, K. S., Miller, C. K., Johnson, G. M., Kleinberg, R. L., and Pennington, W. D.: Seeking the sweet spot: Reservoir and completion quality in organic shales, Oilfield Rev., 25, 16–29, 2014.

Greene, T. J., Carroll, A. R., Wartes, M., Graham, S. A., and Wooden, J. L.: Integrated provenance analysis of a complex orogenic terrane: Mesozoic uplift of the Bogda Shan and inception of the Turpan-Hami Basin, NW China, J. Sediment. Res., 75, 251–267, 2005.

Guo, Z., Zhang, Z., Wu, C., Fang, S., and Zhang, R.: The Mesozoic and Cenozoic exhumation history of Tianshan and comparative studies to the junggar and Altai mountains, Acta Geol. Sin., 80, 1–15, 2006.

Hatch, J. R. and Leventhal, J. S.: Relationship between inferred redox potential of the depositional environment and geochemistry of the Upper Pennsylvanian (Missourian) Stark shale member of the Dennis Limestone, Wabaunsee County, Kansas, USA, Chem. Geol., 99, 65–82, 1992.

Herkat, M. and Ladjal, A.: Paleobathymetry of foraminiferal assemblages from the Pliocene of the Western Sahel (North-Algeria), Palaeogeogr. Palaeocl., 374, 144–163, 2013.

Hu, F., Meng, Q., and Liu, Z.: Mineralogy and element geochemistry of oil shales in the Lower Cretaceous Qingshankou Formation of the southern Songliao Basin, northeast China: implications of provenance, tectonic setting, and paleoenvironment, ACS Earth Space Chem., 5, 365–380, 2021.

Ji, H., Tao, H., Wang, Q., Qiu, Z., Ma, D., Qiu, J., and Liao P.: Early to middle Jurassic tectonic evolution of the Bogda mountains, northwest China: evidence from sedimentology and detrital zircon geochronology, J. Asian Earth Sci., 153, 57–74, 2018.

Jiang, S. H., Li, S. Z., Somerville, I. D., Lei, J. P., and Yang, H. Y.: Carboniferous-Permian tectonic evolution and sedimentation of the Turpan-Hami Basin, NW China: Implications for the closure of the Paleo-Asian Ocean, J. Asian Earth Sci., 113, 644–655, 2015.

Kidder, D. L. and Erwin, D. H.: Secular distribution of biogenic silica through the phanerozoic: Comparison of silica-replaced fossils and bedded cherts at the series level, J. Geol., 109, 509–522, 2001.

Korobkin, V. V. and Buslov, M. M.: Tectonics and geodynamics of the western Central Asian Fold Belt (Kazakhstan Paleozoides), Russ. Geol. Geophys., 52, 1600–1618, 2011.

Taylor, S. R. and McLennan, S. M.: The Continental Crust: Its Composition and Evolution, Blackwell Scientific Publications, Oxford, https://doi.org/10.1017/S0016756800032167, 1985.

Kroonenberg, S. B.: Effect of provenance, sorting and weathering on the geochemistry of fluvial sands from different tectonic and climatic environments, in: Proceedings of the 29th International Geological Congress, Part A, Kyoto, Japan, 24 August–3 September 1992, 69, 81, Kyoto, Japan, 851052, edited by: Kumon, F. and Yu, K. M., 1992.

Lerman, A. and Baccini, P.: Lakes: Chemisty, Geology, Physics, Springer-Verlag, New York, https://doi.org/10.1007/978-1-4757-1152-3. 1978.

Li, C. M., Liu, J. T., Ni, L. B., and Fan, S. W.: Characteristics of deep geological structure and petroleum exploration prospect in Turpan-Hami Basin, China Petroleum Exploration, 26, 44–57, 2021 (in Chinese with English abstract).

Li, L., Qu, Y. Q., Meng, Q. R., and Wu, G. L.: Gravity Flow Sedimentation: Theoretical Studies and Field Identification, Acta Sedimentol. Sin., 29, 677–688, 2011.

Li, R. B.: Filling characteristic and research significance of Permian in Tainan Depression of Tuha Basin, Journal of Jilin University, Earth Science Edition, 49, 1518–1528, https://doi.org/10.13278/j.cnki.jjuese.20180243, 2019.

Li, Y. J., Sun, P. C., Liu, Z. J., Yao, S. Q., Xu, Y. B., and Liu, R.: Geochemistry of the Permian Oil Shale in the Northern Bogda Mountain, Junggar Basin, Northwest China: Implications for Weathering, Provenance, and Tectonic Setting, ACS Earth Space Chem., 4, 1332–1348, 2020.

Li, W., Hu, J., Li, D., Liu, J., Sun, Y., and Liang, J.: Analysis of the late Paleozoic and Mesozoic paleocurrents and It's constructional significance of the northern Bogdashan, Xinjiang, Acta Sedimentol. Sin., 25, 283–292, 2007.

Li, Y. L., Shan, X., Gelwick, K. D., Yu, X. H., Jin, L. N., Yao, Z. Q., Li, S. L., and Yang, S. Y.: Permian mountain building in the bogda mountains of NW China, Int. Geol. Rev., 64, 2048270, https://doi.org/10.1080/00206814.2022.2048270, 2022.

Liu, D., Zhang, C., Yao, E., Song, Y., Jiang, Z., and Luo, Q.: What generated the Late Permian to Triassic unconformities in the southern Junggar Basin and western Turpan Basin; tectonic uplift, or increasing aridity?, Palaeogeogr. Palaeocl., 468, 1–17, 2017.

Liu, D., Kong, X., Zhang, C., Wang, J., Yang, D., Liu, X., Wang, X., and Song, Y.: Provenance and geochemistry of Lower to Middle Permian strata in the southern Junggar and Turpan basins: a terrestrial record from mid-latitude NE Pangea, Palaeogeogr. Palaeocl., 495, 259–277, 2018.

Liu, G. and Zhou, D.: Application of microelements analysis in identifying sedimentary environment-taking Qianjiang Formation in the Jiang Han Basin as a example, Pet. Geo. Exp., 29, 307–311, 2007 (in Chinese with English abstract).

Maravelis, A. G., Offler, R., Pantopoulos, G., and Collins, W. J.: Provenance and tectonic setting of the Early Permian sedimentary succession in the southern edge of the Sydney Basin, eastern Australia, Geol. J., 56, 2258–2276, 2021.

McLennan, S. M., Taylor, S. R., and Kröner, A.: Geochemical evolution of Archean shales from South Africa I: The Swaziland and Ponggola Supergroups, Precambrian Res., 22, 93–124, 1983.

McLennan, S. M., Hemming, S., McDaniel, D. K., and Hanson, G. N.: Geochemical approaches to sedimentation, provenance, and tectonics, Spec. Pap. Geol. Soc. Am., 284, 21–40, 1993.

Mei, X., Li, X. J., Mi, P. P., Zhao, L., Wang, Z. B., Zhong, H. X., Yang, H., Huang, X. T., He, M. Y., Xiong, W., and Zhang, Y.: Distribution regularity and sedimentary differentiation patterns of China seas surface sediments, Geol. China, 47, 1447–1462, 2020 (in Chinese with English abstract).

Miao, H., Wang, Y. B., Zhao, S. H., Guo, J. Y., Ni, X. M., Gong, X, Zhang, Y. J., and Li, J. H.: Geochemistry and Organic Petrology of Middle Per-mian Source Rocks in Taibei Sag, Turpan-Hami Basin, China: Implication for Organic Matter Enrichment, ACS Omega, 6, 31578–31594, 2021.

Miao, H., Wang, Y. B., Guo, J. Y., Fu, Y., and Li, J. H.: Weathering correction and hydrocarbon generation and expulsion potential of Taodonggou Group source rocks in Taibei Sag in Turpan-Hami Basin, Petrol. Geol. Oilfield Dev. Daq., 42, 22–32, 2023.

Miao, H., Wang, Y. B., Guo, J. Y., Han, W. L., and Gong, X.: Evaluation of Middle Permian source rocks of the Taodonggou Group in the Turpan Hami Basin, Geophys. Prospect. Petrol., 61, 733–742, 2022a (in Chinese with English abstract).

Miao, H., Wang, Y. B., He, C., Li, J. H., Zhang, W., Zhang, Y. J., and Gong, X.: Fault development characteristics and reservoir control in Chengbei fault step zone,Bohai Bay Basin, Lithol. Reserv., 34, 105–115, 2022b (in Chinese with an English abstract).

Miao, H., Wang, Y. B., Ma, Z. T., Guo, J. Y., and Zhang, Y. J.: Generalized Deltalog R model with spontaneous potential and its application in predicting total organ carbon content, J. Min. Sci. Technol., 7, 417–426, 2022c (in Chinese with English abstract).

Miao, J. Y., Zhou, L. F., Deng, K., Li, J. F., Han, Z. Y., and Bu, Z. Q.: Organic Matters from Middle Permain Source rocks of Northern Xinjiang and Their Relationships with Sedimentary environments, Geochemica, 6, 551–560, 2004 (in Chinese with English abstract).

Nesbitt, H. W. and Young, G. M.: Prediction of some weathering trends of plutonic and volcanic rocks based on thermodynamic and kinetic considerations, Geochim. Cosmochim. Ac., 48, 1523–1534, 1984.

Novikov, I. S.: Reconstructing the stages of orogeny around the Junggar basin from the lithostratigraphy of Late Paleozoic, Mesozoic, and Cenozoic sediments, Russ. Geol. Geophys., 54, 138–152, 2013.

Obrist-Farner, J., Yang, W., and Hu, X. F.: Nonmarine time-stratigraphy in a rift setting: an example from the Mid-Permian lower Quanzijie low-order cycle Bogda Mountains, NW China, J. Palaeogeogr., 4, 27–51, 2015.

Pinto, L., Munoz, C., Nalpas, T., and Charrier, R.: Role of sedimentation during basin inversion in analogue modelling, J. Struct. Geol., 32, 554–565, 2010.

Rollinson, H. R.: Using Geochemical Data: Evaluation, Presentation, Interpretation, Longman Scientific Technical, New York, https://doi.org/10.4324/9781315845548, 1993.

Rosenthal, Y., Lam, P., Boyle, E. A., and Thomson, J.: Authigenic cadmium enrichments in suboxic sediments: precipitation and postdepositional mobility – sciencedirect, Earth Planet. Sc. Lett., 132, 99–111, 1995.

Roser, B. P. and Korsch, R. J.: Provenance Signatures of Sandstone-mudstone suites determined using discriminant functiom analysis of major-element data, Chem. Geol., 67, 119–139, 1988.

Ross, D. J. K. and Bustin, R. M.: Investigating the use of sedimentary geochemical proxies for paleoenvironment interpretation of thermally mature organic-rich strata: Examples from the Devonian–Mississippian shales, Western Can. Sediment. Basin Chem. Geol., 260, 1–19, 2009.

Schoepfer, S. D., Shen, J., Wei, H. Y., Tyson, R. V., Ingall, E., and Algeo, T. J.: Total organic carbon, organic phosphorus, and biogenic barium fluxes as proxies for paleomarine productivity, Earth Sci. Rev., 149, 23–52, 2015.

Shao, L., Li, W. H., and Yuan, M. S.: Characteristic of sandstone and its tectonic implications of the Turpan Basin, Acta Sediment. Sin., 17, 435–441, 1999.

Shao, L., Stattegger, K., and Garbe-Schoenberg, C.: Sandstone petrology and geochemistry of the Turpan Basin (NW China): implications for the tectonic evolution of a Continental Basin, J. Sediment. Res., 71, 37–49, 2001 (in Chinese with English abstract).

Shi, J., Zou, Y. R., Cai, Y. L., Zhan, Z. W., Sun, J. N., Liang, T., and Peng, P. A.: Organic matter enrichment of the Chang 7 member in the Ordos Basin: Insights from chemometrics and element geochemistry, Mar. Petrol. Geol., 134, 105306, https://doi.org/10.1016/j.marpetgeo.2021.105404, 2021.

Shi, Y. Q, Ji, H. C., Yu, J. W, Xiang, P. F., Yang, Z. B., and Liu, D. D.: Provenance and sedimentary evolution from the Middle Permian to Early Triassic around the Bogda Mountain, NW China: A tectonic inversion responding to the consolidation of Pangea, Mar. Pet. Geol., 114, 104169, https://doi.org/10.1016/j.marpetgeo.2021.105404, 2020.

Shu, L., Wang, B., Zhu, W., Guo, Z., Charvet, J., and Zhang, Y.: Timing of initiation of extension in the Tianshan, based on structural, geochemical and geochronological analyses of bimodal volcanism and olistostrome in the Bogda Shan (NW China), Int. J. Earth Sci., 100, 1647–1663, 2011.

Song, J., Bao, Z., Zhao, X. M., Gao, Y. S., Song, X. M., Zhu, Y. Z., Deng, J., Liu, W., Wang, Z. C., Ming, C. D., Meng, Q. K., Zhang, L., Mao, S. W., Zhang, Y. L., Yu, X., and Wei, M. Y.: Sedimentology and geochemistry of Middle–Upper Permian in northwestern Turpan–Hami Basin, China: Implication for depositional environments and petroleum geology, Energ. Explor. Exploit., 36, 910–941, 2018.

Sun, G. and Liu, Y.: The preliminary analysis of the uplift time of Bogda Mountain, Xinjiang, Northwest China, Acta Sedimentol. Sin., 27, 487–491, 2009.

Tang, W., Zhang, Z., Li, J., Li, K., Chen, Y., and Guo, Z.: Late Paleozoic to Jurassic tectonic evolution of the Bogda area (northwest China): evidence from detrital zircon U–Pb geochronology, Tectonophysics, 626, 144–156, 2014.

Taylor, S. R. and Mclennan, S. M.: The continental crust: Its composition and evolution, Blackwell Science Publications, Oxford, https://doi.org/10.1017/S0016756800032167, 1985.

Thorpe, C. L., Law, G. T. W., Boothman, C., Lloyd, J. R., Burke, I. T., and Morris, K.: The Synergistic Effects of High Nitrate Concentrations on Sediment Bioreduction, Geomicrobiol. J., 29, 484–493, 2012.

Tian, J. Q., Liu, J. Z., Zhang, Z. B., and Cong, F. Y.: Hydrocarbon-generating potential, depositional environments, and organisms of the Middle Permian Tarlong Formation in the Turpan-Hami Basin, northwestern China, GSA Bull., 129, 1252–1265, 2017.

Tribovillard, N. P., Desprairies, A., Lallier?verges, E., Bertrand, P., Moureau, N., Ramdani, A., and Ramanampiso, L.: Geochemical study of organic-matter rich cycles from the Kimmeridge Clay Formation of Yorkshire (UK): productivity versus anoxia, Palaeogeogr. Palaeocl., 108, 165–181, 1994.

Tribovillard, N., Algeo, T. J., Lyons, T., and Riboulleau, A.: Trace metals as paleoredox and paleoproductivity proxies: an update, Chem. Geol., 232, 12–32, 2006.

Tribovillard, N., Algeo, T. J., Baudin, F., and Riboulleau, A.: Analysis of marine environmental conditions based on molybdenum–uranium covariation – applications to Mesozoic paleoceanography, Chem. Geol., 324, 46–58, 2012.

Wartes, M. A., Carroll, A. R., and Greene, T. J.: Permian sedimentary record of the Turpan-Hami basin and adjacent regions, northwest China: Constraints on postamalgamation tectonic evolution, Geol. Soc. Am. Bull., 114, 131–152, 2002.

Wang, A., Wang, Z., Liu, J., Xu, N., and Li, H.: The Sr / Ba ratio response to salinity in clastic sediments of the Yangtze River Delta, Chem. Geol., 559, 119923, https://doi.org/10.1016/j.chemgeo.2020.119923, 2021.

Wang, J., Cao, Y. C., Wang, X. T., Liu, K. Y., Wang, Z. K., and Xu, Q. S.: Sedimentological constraints on the initial uplift of the West Bogda Mountains in Mid-Permian, Sci. Rep., 8, 1453, https://doi.org/10.1038/s41598-018-19856-3, 2018a.

Wang, J., Wu, C., Li, Z., Zhu, W., Zhou, T., Wu, J., and Wang, J.: The tectonic evolution of the Bogda region from Late Carboniferous to Triassic time: evidence from detrital zircon U–Pb geochronology and sandstone petrography, Geol. Mag., 155, 1063–1088, 2018b.

Wang, J., Wu, C., Zhou, T., Zhu, W., Zhou, Y., Jiang, X., and Yang, D.: Source-to-Sink analysis of a transtensional rift Basin from syn-rift to uplift stages, J. Sediment. Res., 89, 335–352, 2019.

Wang, J. L., Wu, C. D., Zhou, T. Q., Zhu, W., Li, X. Y., and Zhang, T.: Source and sink evolution of a Permian–Triassic rift–drift basin in the southern Central Asian Orogenic Belt: Perspectives on sedimentary geochemistry and heavy mineral analysis, J. Asian Earth Sci., 181, 103905, https://doi.org/10.1016/j.jseaes.2019.103905, 2019.

Wang, L.: Sediment flux and mechanism for the uplifting of the mountain system around the Junggar inland basin Sediment, Geol. Tethyan Geol., 16, 39–46, 1996.

Wang, Y.: Mixed Sedimentary Characteristics and Pattern of the Fan Delta in the Middle Permian Taerlanggou Profile, Xinjiang Province Acta Sediment. Sin., 37, 922–933, 2019 (in Chinese with English abstract).

Wang, Z. W., Yu, F., Wang, J., Fu, X. G., Chen, W. B., Zeng, S. Q., and Song, C. Y.: Palaeoenvironment evolution and organic matter accumulation of the Upper Triassic mudstone from the eastern Qiangtang Basin (Tibet), eastern Tethys, Mar. Petrol. Geol., 130, 105113, https://doi.org/10.1016/j.marpetgeo.2021.105113, 2021.

Wronkiewicz, D. J. and Condie, K. C.: Geochemistry of archean shales from the witwatersrand supergroup, south Africa: Source-area weathering and provenance, Geochim. Cosmochim. Ac., 51, 2401–2416, 1987.

Wei, H., Chen, D. Z., Wang, J. G., Yu, H., and Tucker, M. E.: Organic accumulation in the lower Chihsia Formation (Middle Per-

mian) of South China: Constraints from pyrite morphology and multiple geochemical proxies, Palaeogeogr. Palaeocl., 353, 73–86, 2012.

Wei, X. X.: Middle-Late Permian fossil woods from Northern Tuha Basin: Implications for Palaeoclimate, MS thesis, Wuhan, China university of Geosciences, 2015 (in Chinese with English abstract).

Wu, C., Li, H. W., Sheng, S. Z., Chen, T., Shi, X. F., and Jiang, M. L.: Characteristics and main controlling factors of hydrocarbon accumulation of Permian-Triassic in Lukeqin structural zone, Tuha Basin, China Petrol. Explor., 26, 137–148, 2021 (in Chinese with English abstract).

Xiong, X. H. and Xiao, J. F.: Geochemical Indicators of Sedimentary Environments – A Summary, Earth Environ., 39, 405–414, 2011 (in Chinese with English abstract).

Xu, C., Shan, X. L., Lin, H. M., Hao, G. L., Liu, P., Wang, X. D., Shen, M. R., Rexiti, Y., Li, K., Li, Z. S., Wang, X. M., Du, X. D., Zhang, Z. W., Jia, P. M., and He, W. T.: The formation of early Eocene organic-rich mudstone in the western Pearl River Mouth Basin, South China: Insight from paleoclimate and hydrothermal activity, Int. J. Coal Geol., 253, 103957, https://doi.org/10.1016/j.coal.2022.103957, 2022.

Xu, H. Y.: Characteristics of Permian Dark Fine-Grained Sedimentary rocks and their shale oil and gas Sigificance in the Northern Margin of Turpan-Hami Basin, MS thesis, Xi'an: Chang'an University, 2022 (in Chinese with English abstract).

Yang, W., Feng, Q., Liu, Y. Q., Tabor, N., Miggins, D., Crowley, J. L., Lin, J. Y., and Thomas, S.: Depositional environments and cyclo- and chronostratigraphy of uppermost Carboniferous–Lower Triassic fluvial–lacustrine deposits, southern Bogda Mountains, NW China – A terrestrial paleoclimatic record of mid-latitude NE Pangea, Glob. Planet. Change, 73, 15–113, 2010.

Yang, Y., Song, C., and He, S.: Jurassic tectonostratigraphic evolution of the Junggar basin, NW China: a record of Mesozoic intraplate deformation in Central Asia, Tectonics, 34, 86–115, 2015.

You, J., Liu, Y., Zhou, D., Zheng, Q., Vasichenko, K., and Chen, Z.: Activity of hydrothermal fluid at the bottom of a lake and its influence on the development of high-quality source rocks: Triassic Yanchang Formation, southern Ordos Basin, China, Austr. J. Earth Sci., 67, 115–128, 2019.

Yu, Y., Cai, H. L., Yin, T. J., Zhang, X. Q., Xu, H., Huang, Y. R., and Cao, T. T.: Sedimentary Characteristics and Depositional Model of Lacustrine Gravity Flow Deposits: A case study of the Cretaceous Pointe Indienne Formation of Block A, Lower Congo Basin, Acta Sediment. Sin., 40, 34–46, 2022.

Zhang, C., He, D., Wu, X., Shi, X., Luo, J., Wang, B., Yang, G, Guan, S., and Zhao, X.: Formation and evolution of multicycle superimposed basins in Junggar Basin, China Petrol. Exp., 11, 47–58, 2006.

Zhang, K., Song, Y., Jiang, S., Jiang, Z. X., Jia, C. Z., Huang, Y. Z., Wen, M., Liu, W. W., Xie, X. L., Liu, T. L., Wang, P. F., Shan, C. A., and Wu, Y. H.: Mechanism analysis of organic matter enrichment in different sedimentary backgrounds: A case study of the Lower Cambrian and the Upper Ordovician-Lower Silurian, in Yangtze region, Mar. Petrol. Geol., 99, 488–497, 2019.

Zhang, S., Liu, C., Bai, J., Wang, J., Ma, M., Guan, Y., and Peng, H.: Provenance variability of the Triassic strata in the Turpan-Hami basin: detrital zircon record of Indosinian tectonic reactivation in eastern Tianshan, Acta Geol. Sin., 93, 1850–1868, 2019.

Zhang, S. C., Zhang, B. M., Bian, L. C., Jing, Z. J., Wang, D. R., Zhang, X. Y., Gao, Z. Y., and Chen, J. F.: Development constraints of marine source rocks in China, Earth Sci. Front., 12, 39–48, 2005 (in Chinese with English abstract).

Zhao, B. S., Li, R. X., Qin, X. L., Wang, N., Zhou, W., Khaled, A., Zhao, D., Zhang, Y. N., Wu, X. L., and Liu, Q.: Geochemical characteristics and mechanism of organic matter accumulation of marine-continental transitional shale of the lower permian Shanxi Formation, southeastern Ordos Basin, north China, J. Petrol. Sci. Eng., 205, 108815, https://doi.org/10.1016/j.petrol.2021.108815, 2021.

Zhao, R., Zhang, J. Y., Zhou, C. M., Zhang, Z. J., Chen, S., Stockli, D.F., Olariu, C., Steel, R., and Wang, H.: Tectonic evolution of Tianshan-Bogda-Kelameili mountains, clastic wedge basin infill and chronostratigraphic divisions in the source-to-sink systems of Permian-Jurassic, southern Junggar Basin, Mar. Petrol. Geol., 114, 104200, https://doi.org/10.1016/j.marpetgeo.2019.104200, 2020.

Zhu, X., Wang, B, Chen, Y., and Liu, H. S.: Constraining the Intracontinental Tectonics of the SW Central Asian Orogenic Belt by the Early Permian Paleomagnetic Pole for the Turfan-Hami Block, J. Geophys. Res.-Sol. Ea., 124, 12366–12387, 2019.